Supporting Information for:

Discovery of New Potent Positive Allosteric Modulators of Dopamine D_2 Receptors: Insights into the Bioisosteric Replacement of Proline to 3-Furoic Acid in the Melanostatin Neuropeptide

Ivo E. Sampaio-Dias,*[,a] Ana Reis-Mendes,[b] Vera Marisa Costa,[b] Xerardo García-Mera,[c] José Brea,[d] María Isabel Loza,[d] Beatriz L. Pires-Lima,[a] Cristina Alcoholado,[e] Manuel Algarra,[f] and José E. Rodríguez-Borges[a]

[a]*LAQV/REQUIMTE, Department of Chemistry and Biochemistry, Faculty of Sciences, University of Porto, 4169-007 Porto, Portugal.*

[b]*UCIBIO, REQUIMTE, Laboratory of Toxicology, Faculty of Pharmacy, University of Porto, 4050-313, Porto, Portugal.*

[c]*Department of Organic Chemistry, Faculty of Pharmacy, University of Santiago de Compostela, E-15782 Santiago de Compostela, Spain.*

[d]*Innopharma Screening Platform. Biofarma Research group. Centre of Research in Molecular Medicine and Chronic Diseases (CIMUS), University of Santiago de Compostela, E-15782 Santiago de Compostela, Spain.*

[e]*Department of Cellular Biology, Genetics and Physiology, Faculty of Sciences, University of Málaga, Campus de Teatinos, 29071 Málaga, Spain.*

[f]*Department of Inorganic Chemistry, Faculty of Sciences, University of Málaga, Campus de Teatinos, 29071 Málaga, Spain.*

*__Corresponding author e-mail__:
idias@fc.up.pt (Ivo E. Sampaio-Dias)

Table of contents

1. NMR spectra

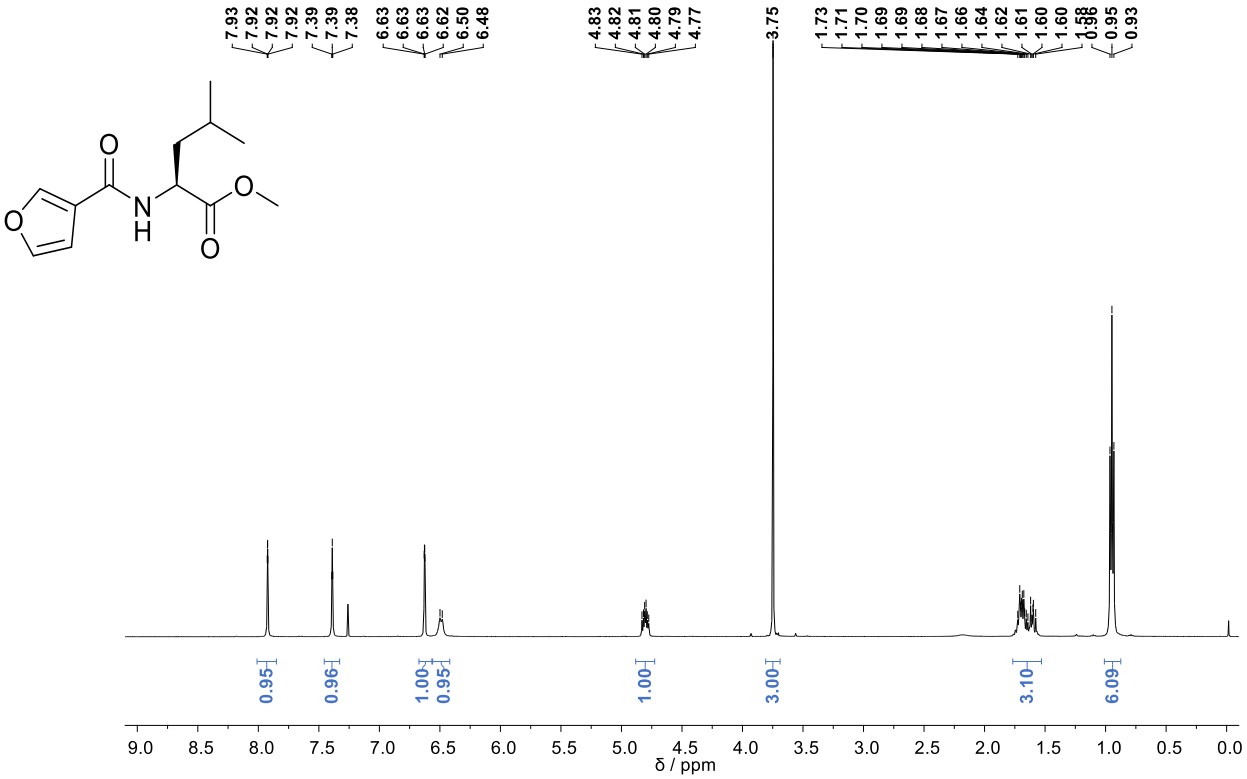

Figure S1. ^{1}H NMR spectrum ($CDCl_3$, 400 MHz) of **2a**.

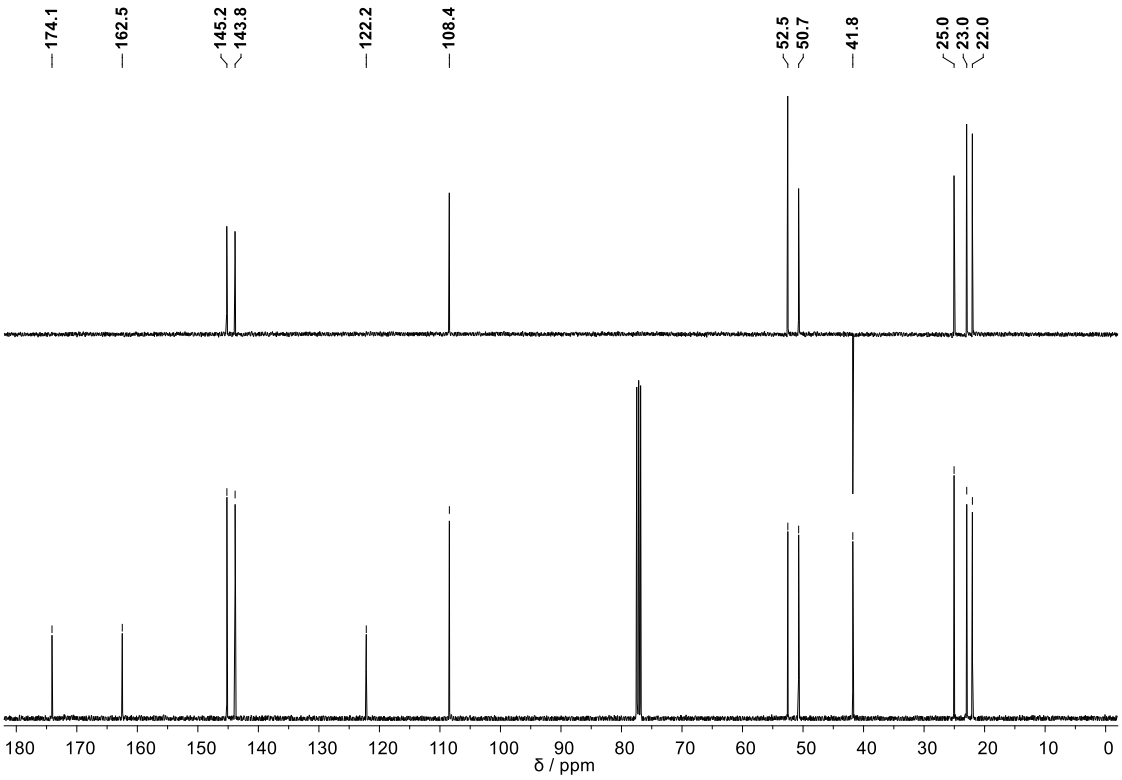

Figure S2. $^{13}C\{^{1}H\}$ NMR and DEPT-135 spectra ($CDCl_3$, 100 MHz) of **2a**.

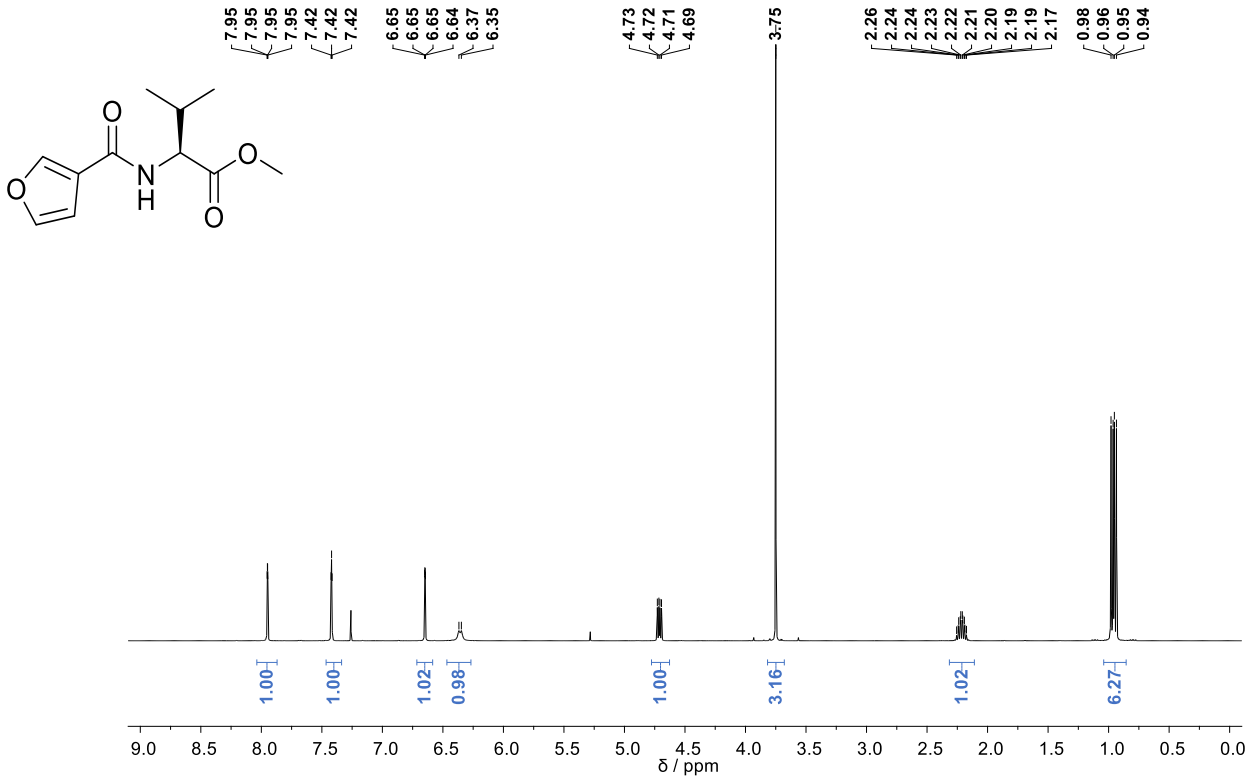

Figure S3. ^{1}H NMR spectrum ($CDCl_3$, 400 MHz) of **2b**.

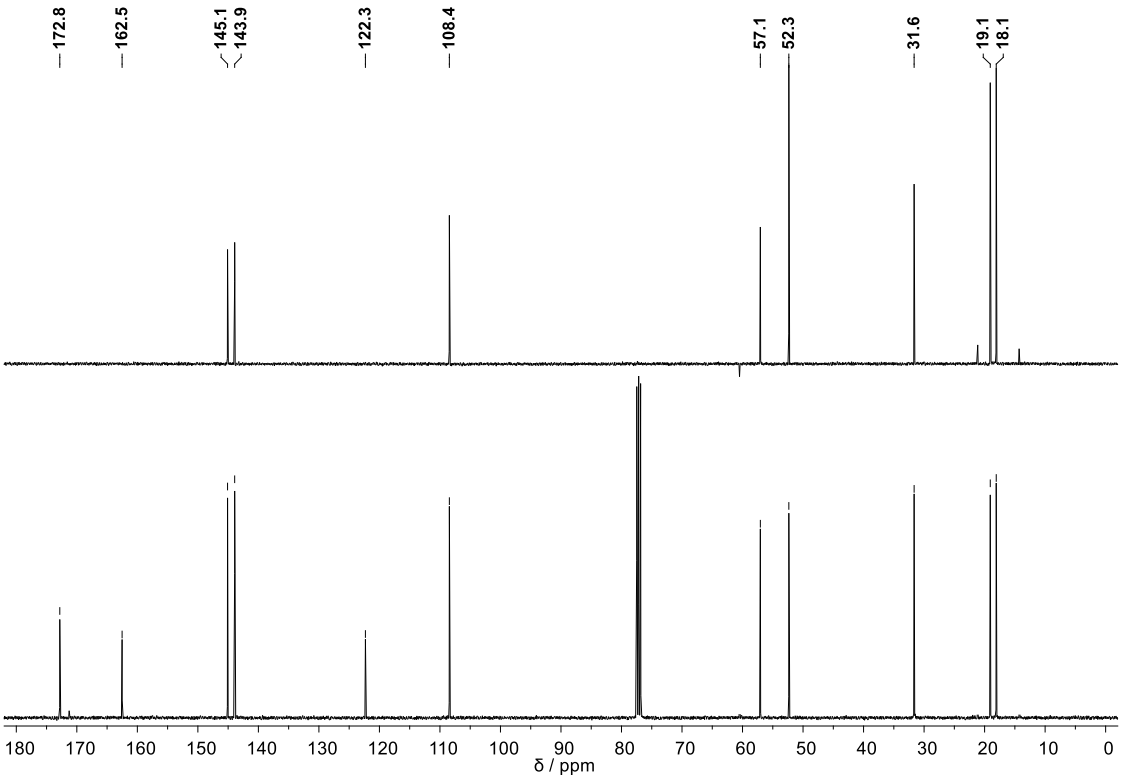

Figure S4. $^{13}C\{^{1}H\}$ NMR and DEPT-135 spectra ($CDCl_3$, 100 MHz) of **2b**.

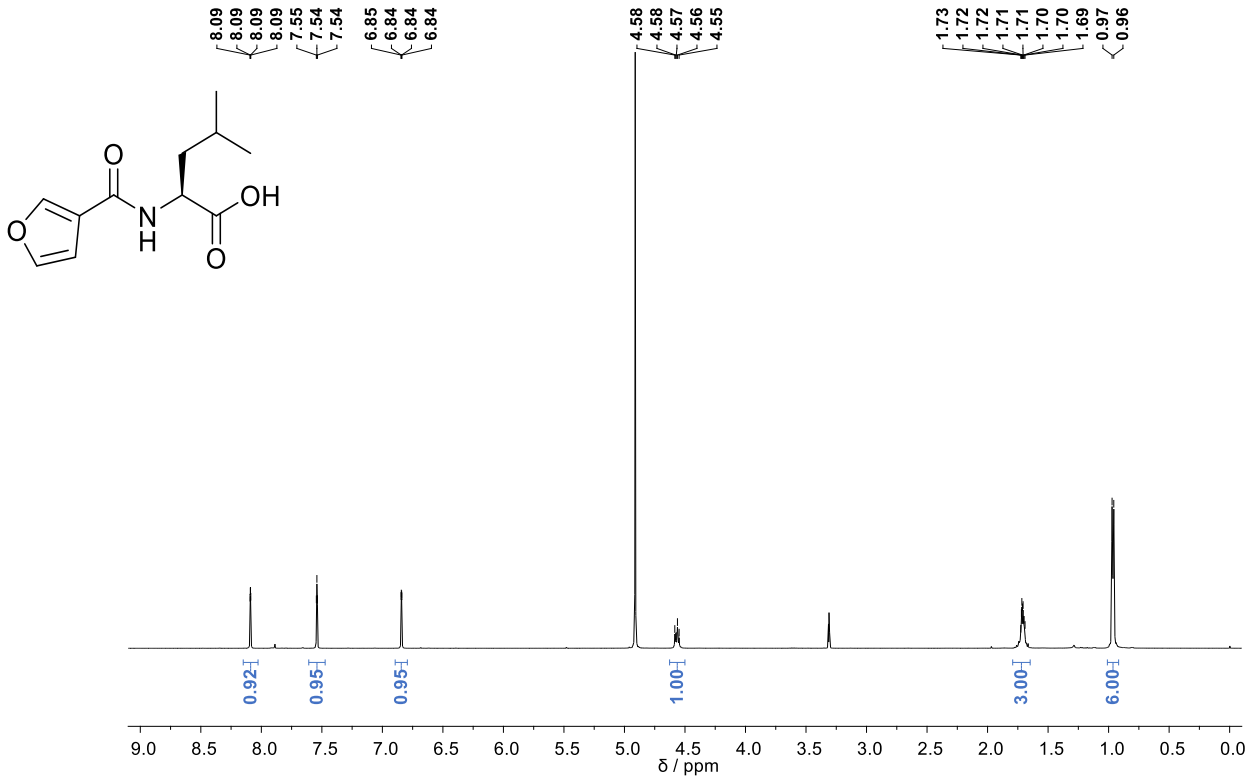

Figure S5. ^{1}H NMR spectrum (CD_3OD, 400 MHz) of **3a**.

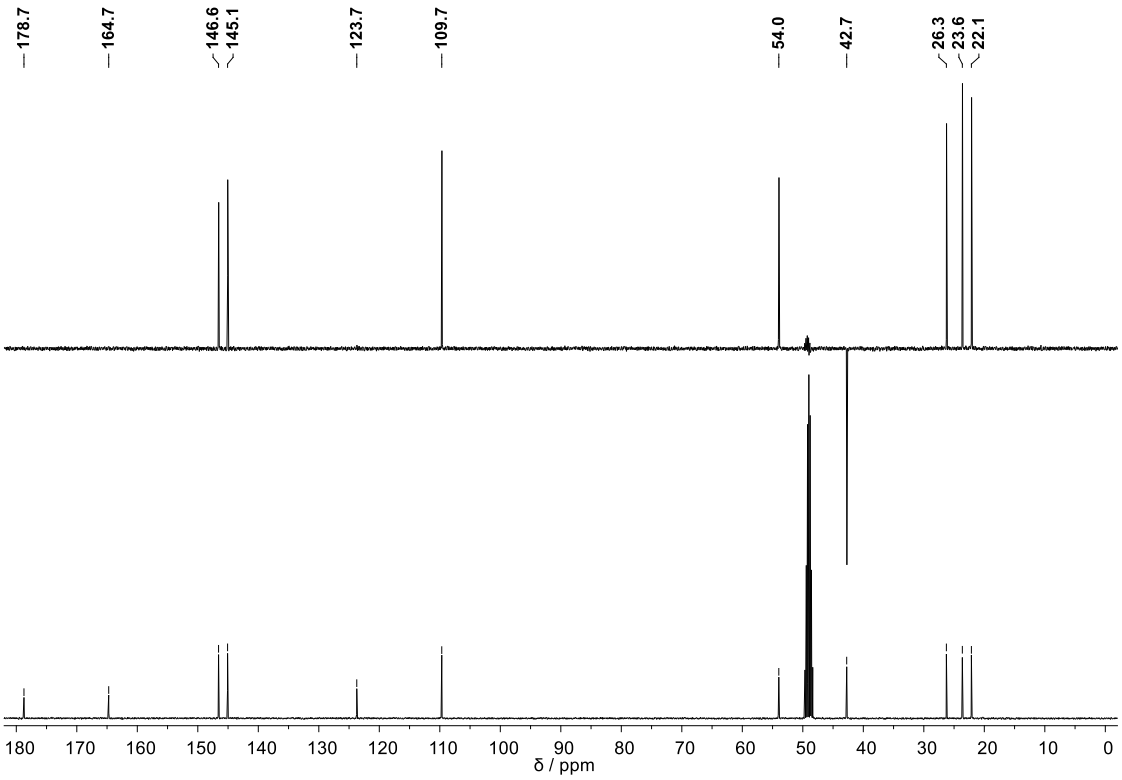

Figure S6. $^{13}C\{^{1}H\}$ NMR and DEPT-135 spectra (CD_3OD, 100 MHz) of **3a**.

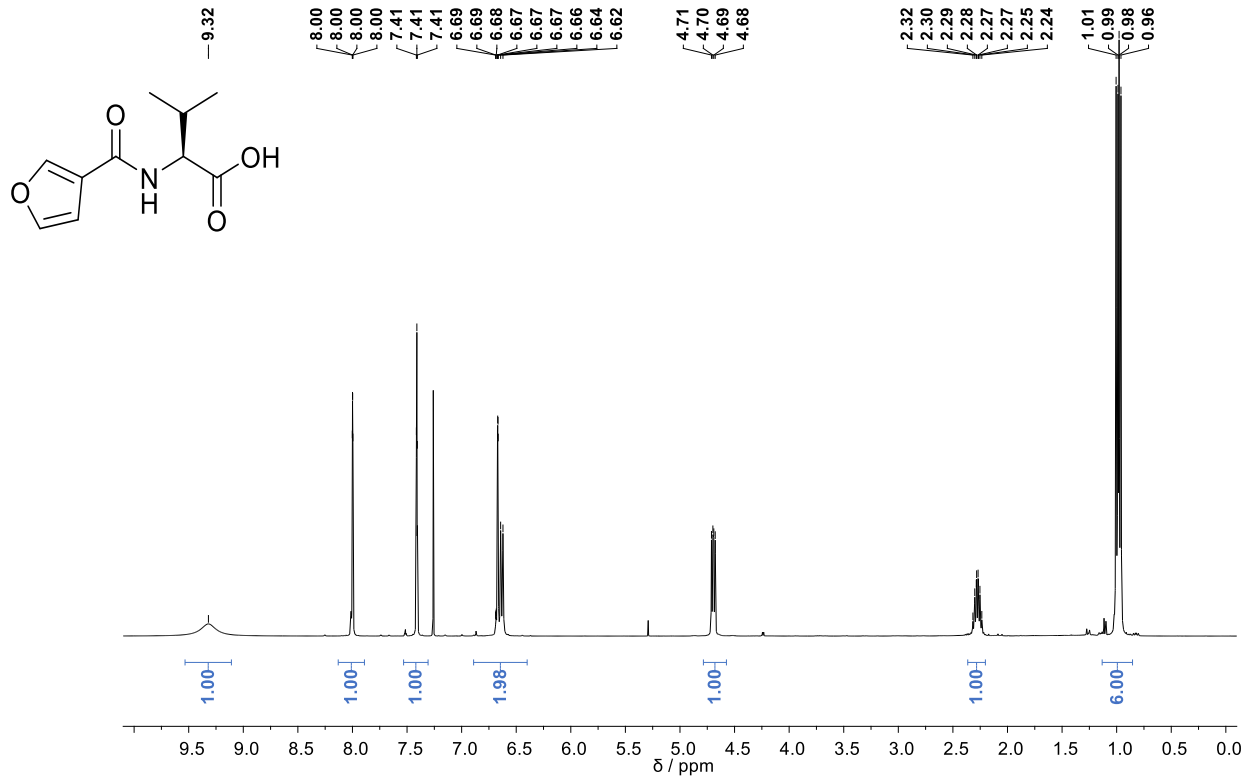

Figure S7. ^{1}H NMR spectrum ($CDCl_3$, 400 MHz) of **3b**.

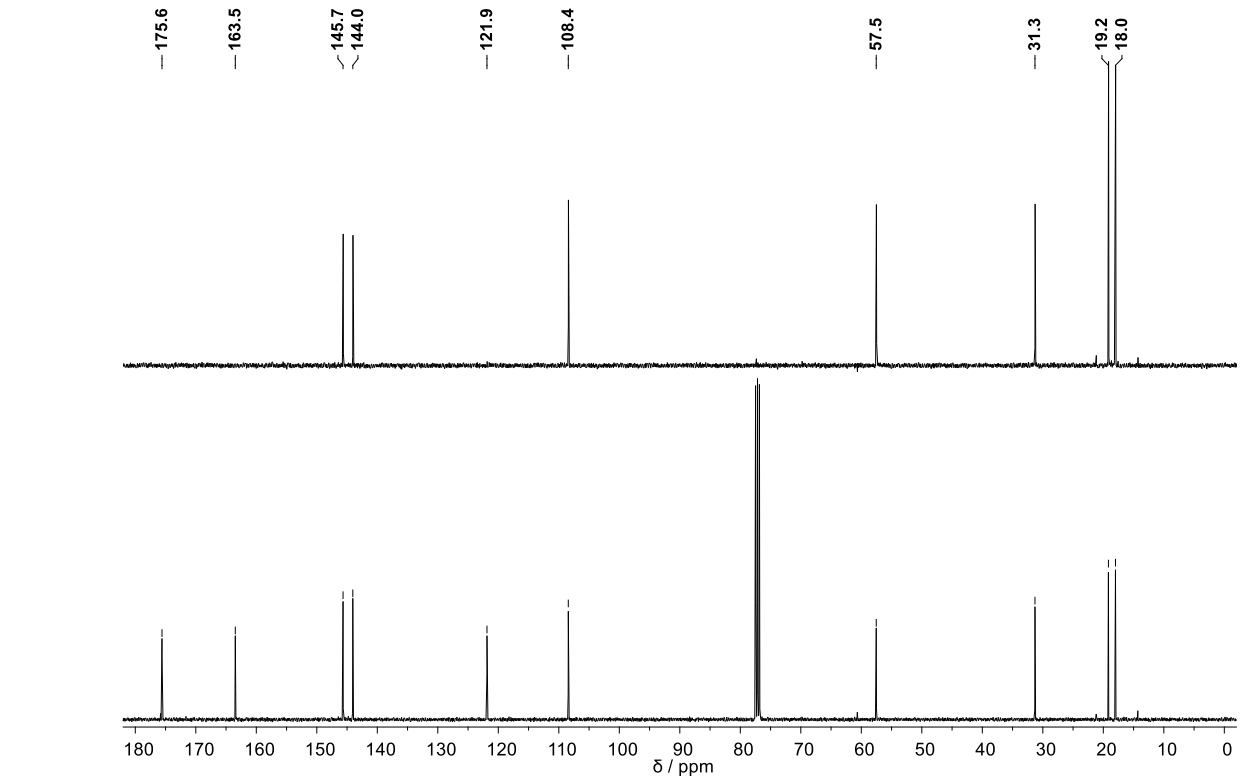

Figure S8. $^{13}C\{^{1}H\}$ NMR and DEPT-135 spectra ($CDCl_3$, 100 MHz) of **3b**.

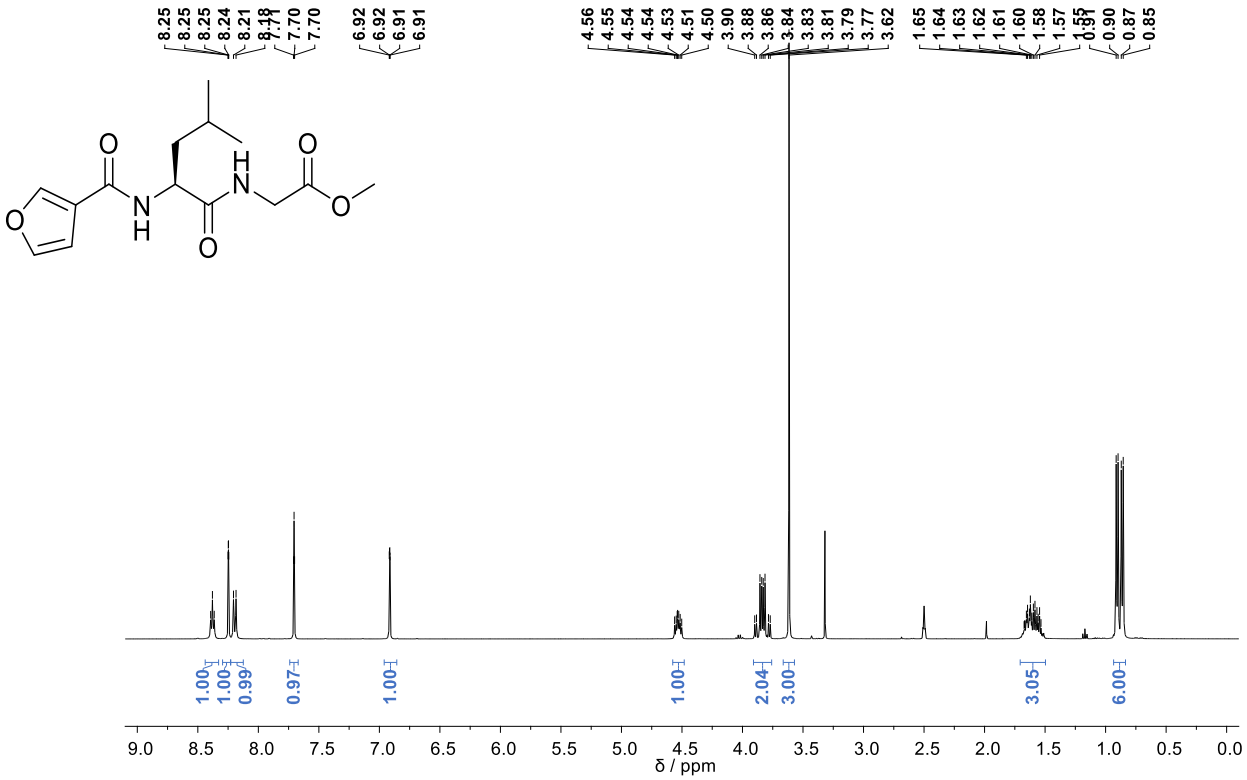

Figure S9. ^{1}H NMR spectrum (DMSO-d_6, 400 MHz) of **4a**.

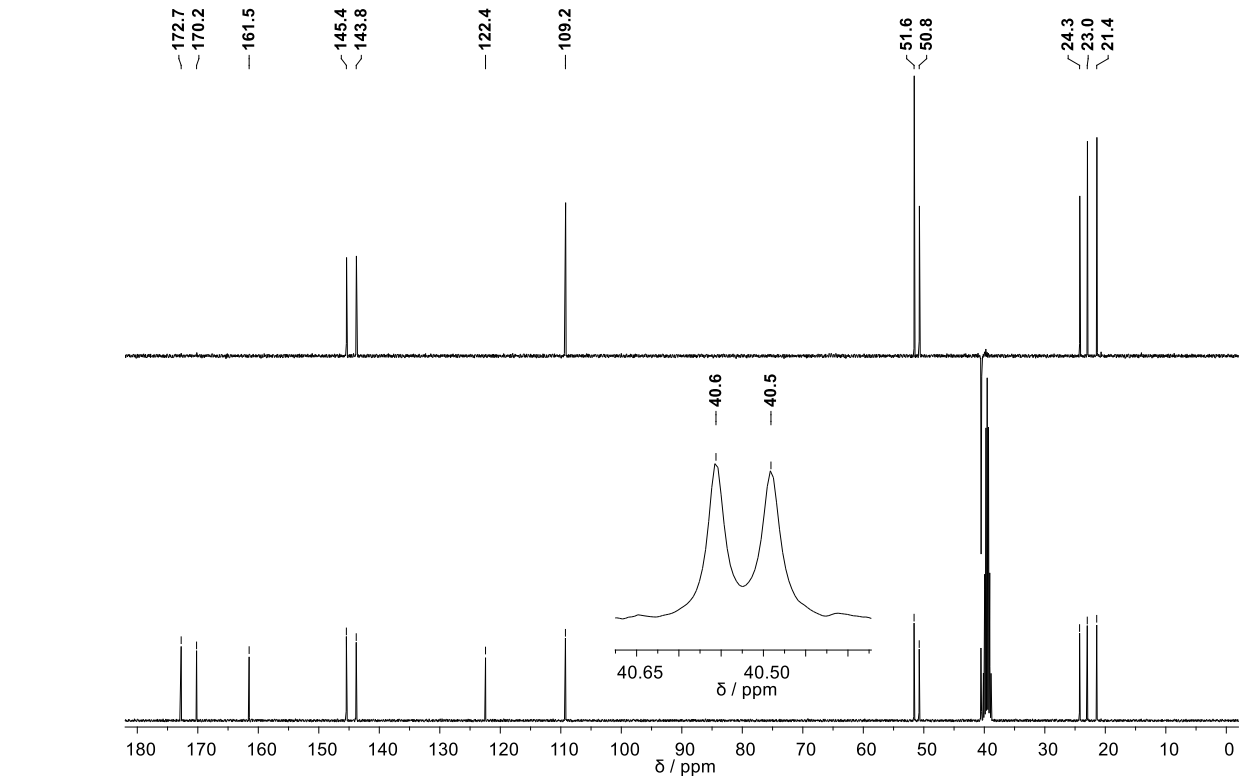

Figure S10. ^{13}C{^{1}H} NMR and DEPT-135 spectra (DMSO-d_6, 100 MHz) of **4a**.

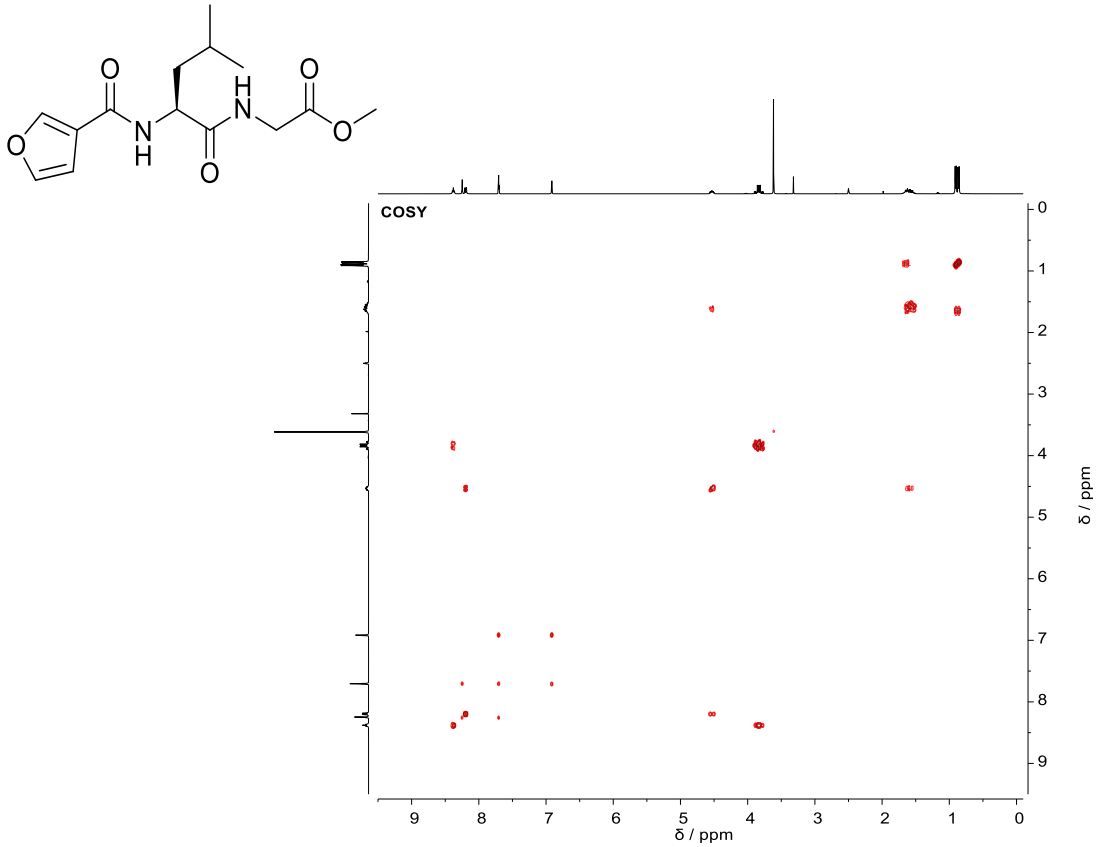

Figure S11. COSY spectrum (DMSO-d_6, 400 MHz) of **4a**.

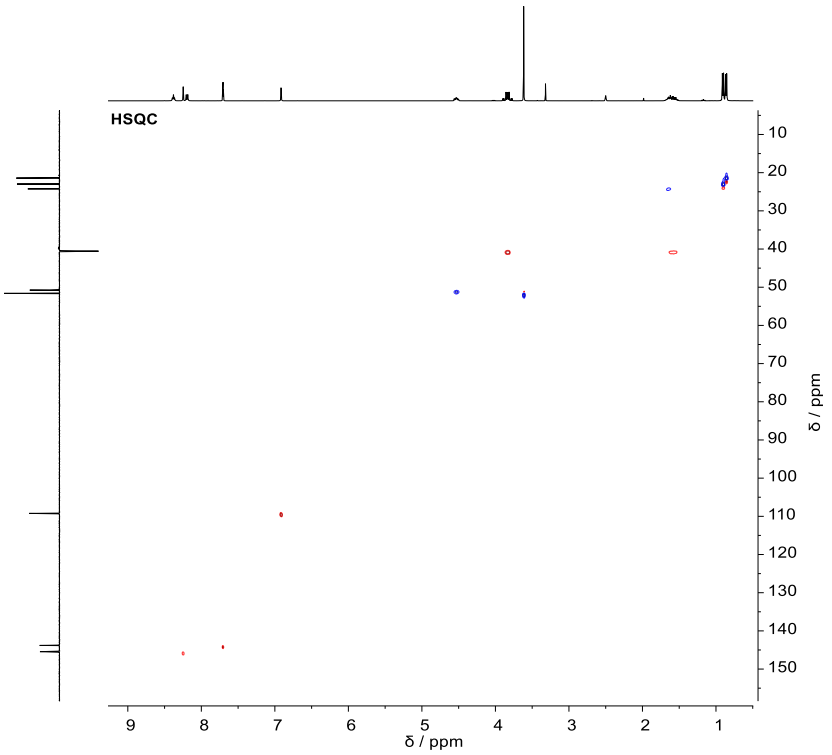

Figure S12. HSQC spectrum (DMSO-d_6, 400 MHz) of **4a**.

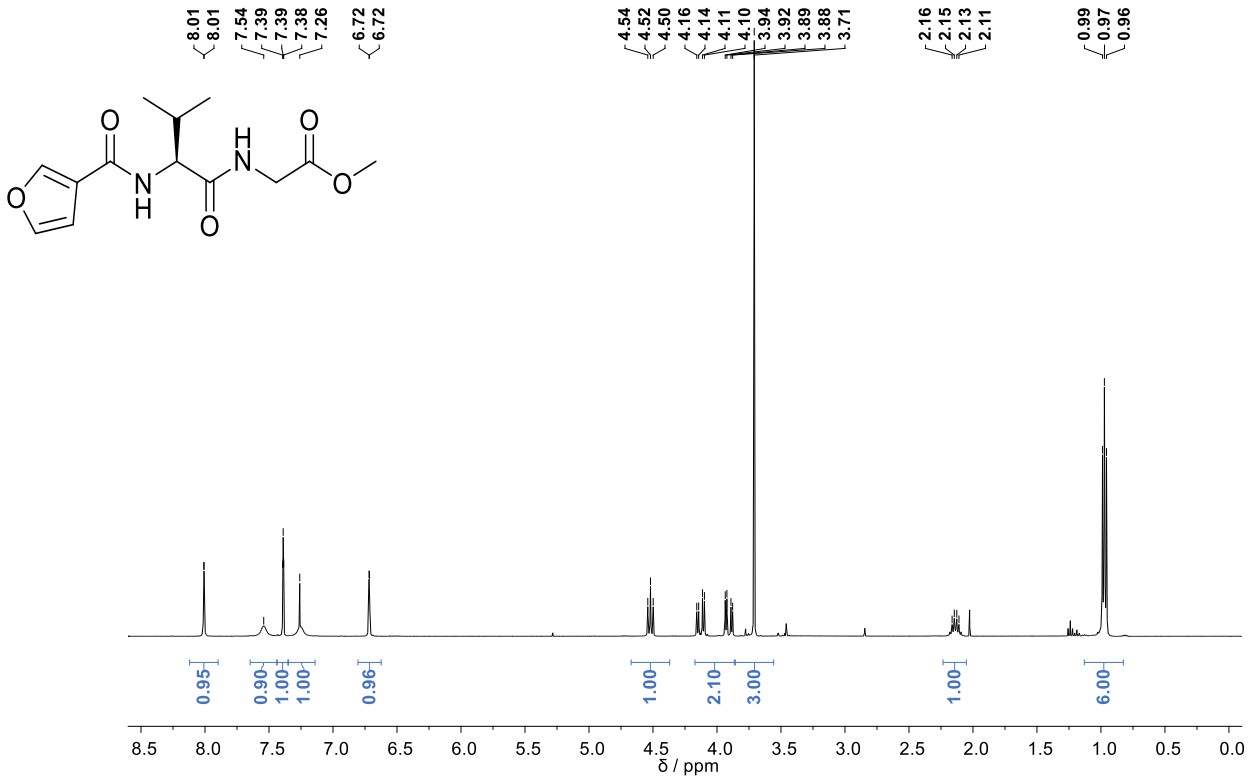

Figure S13. ^{1}H NMR spectrum ($CDCl_3$, 400 MHz) of **4b**.

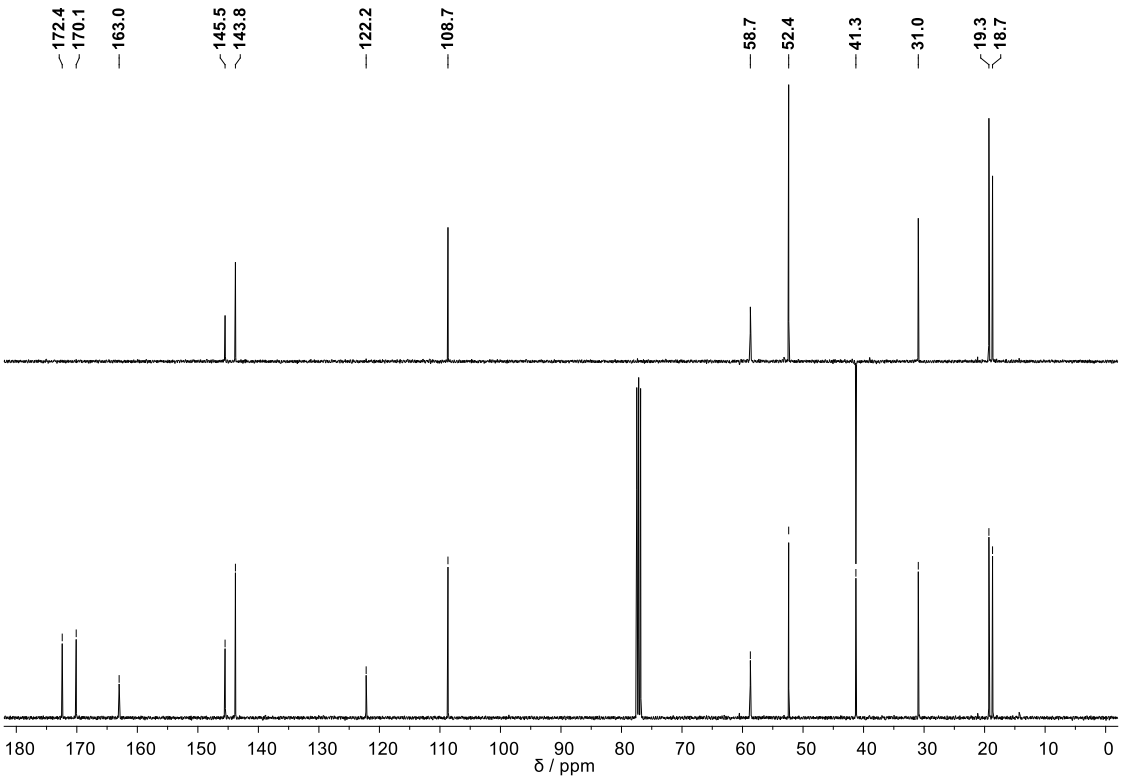

Figure S14. $^{13}C\{^{1}H\}$ NMR and DEPT-135 spectra ($CDCl_3$, 100 MHz) of **4b**.

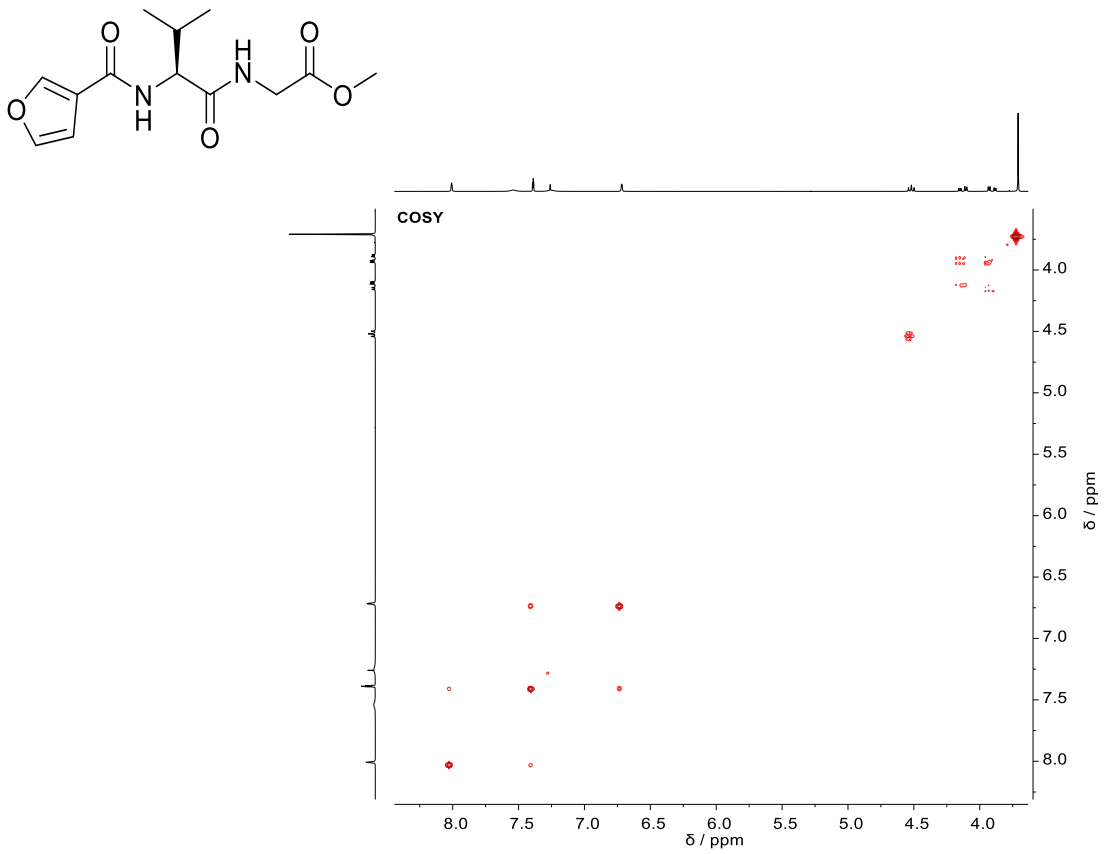

Figure S15. COSY spectrum ($CDCl_3$, 400 MHz) of **4b**.

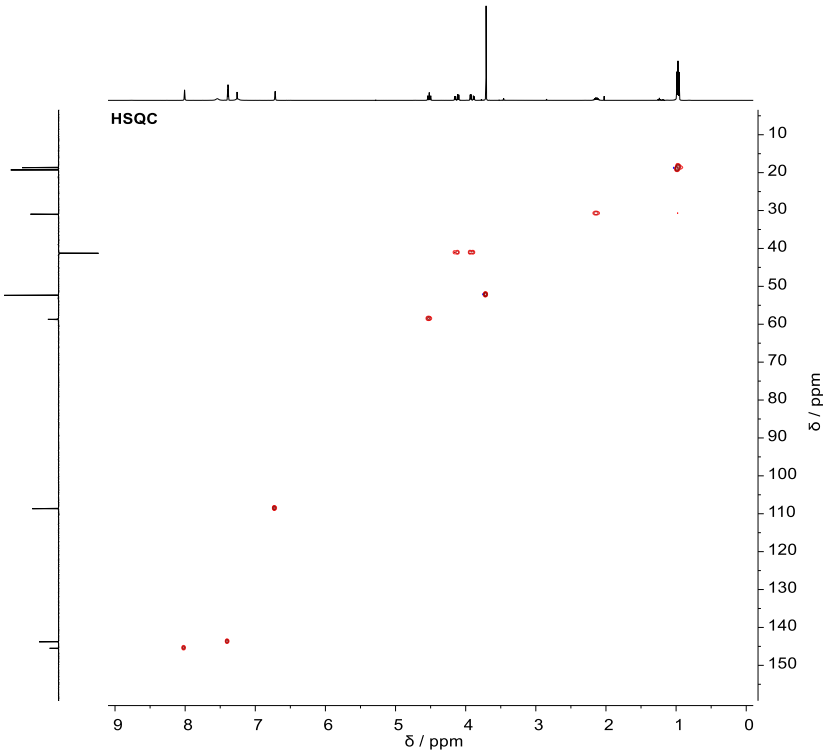

Figure S16. HSQC spectrum ($CDCl_3$, 400 MHz) of **4b**.

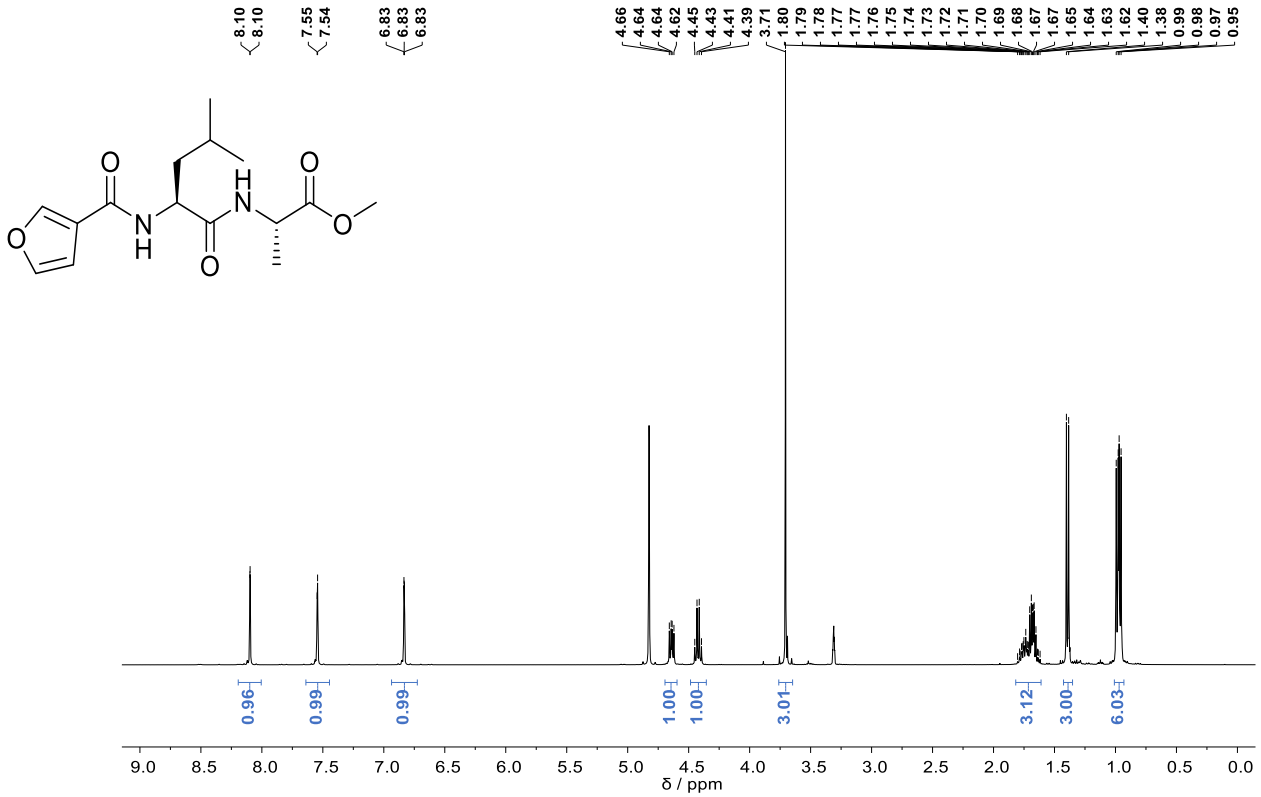

Figure S17. ^{1}H NMR spectrum (CD_3OD, 400 MHz) of **5a**.

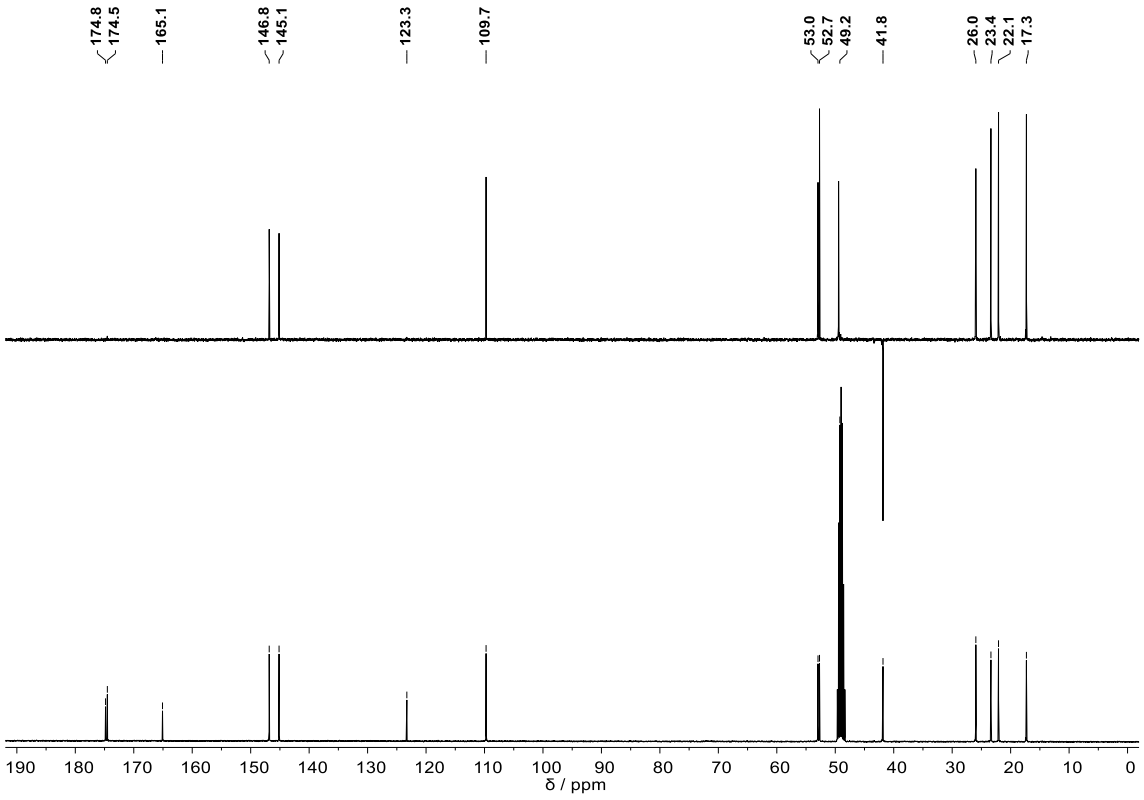

Figure S18. $^{13}C\{^{1}H\}$ NMR and DEPT-135 spectra (CD_3OD, 100 MHz) of **5a**.

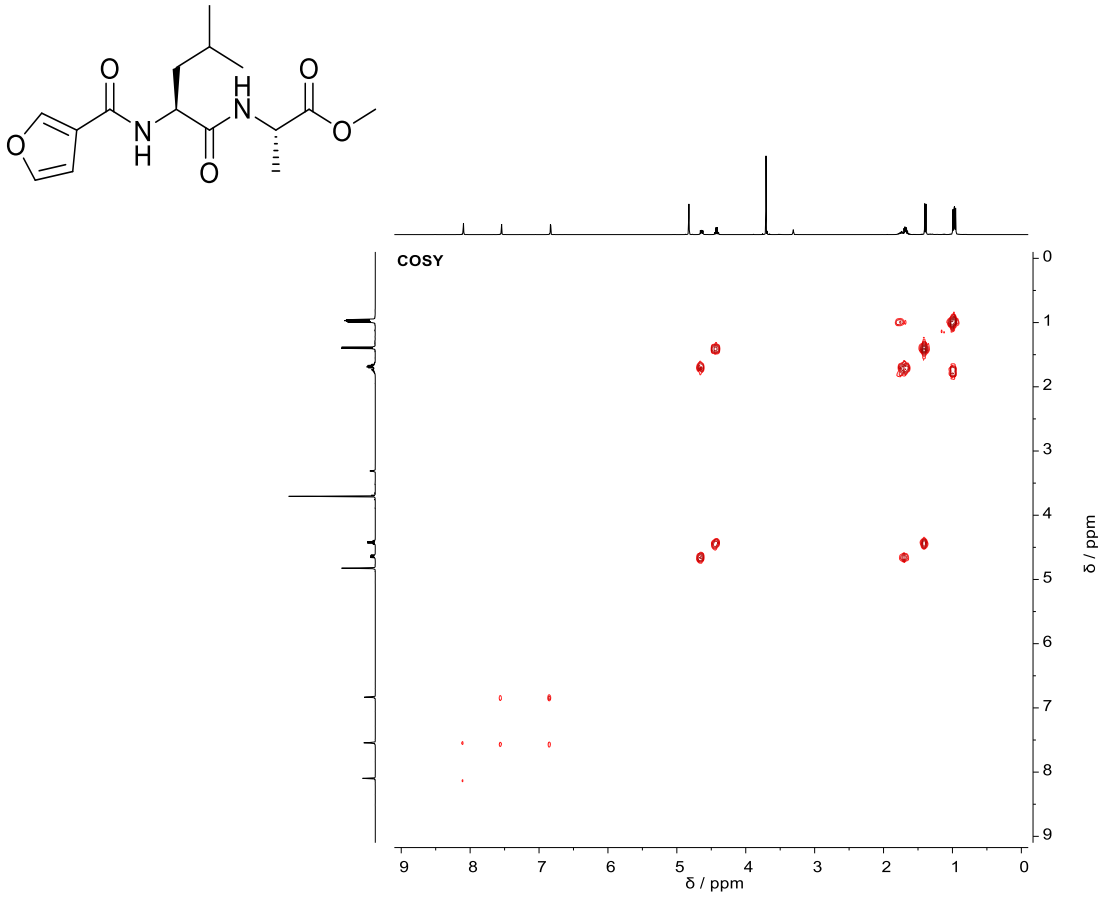

Figure S19. COSY spectrum (CD_3OD, 400 MHz) of **5a**.

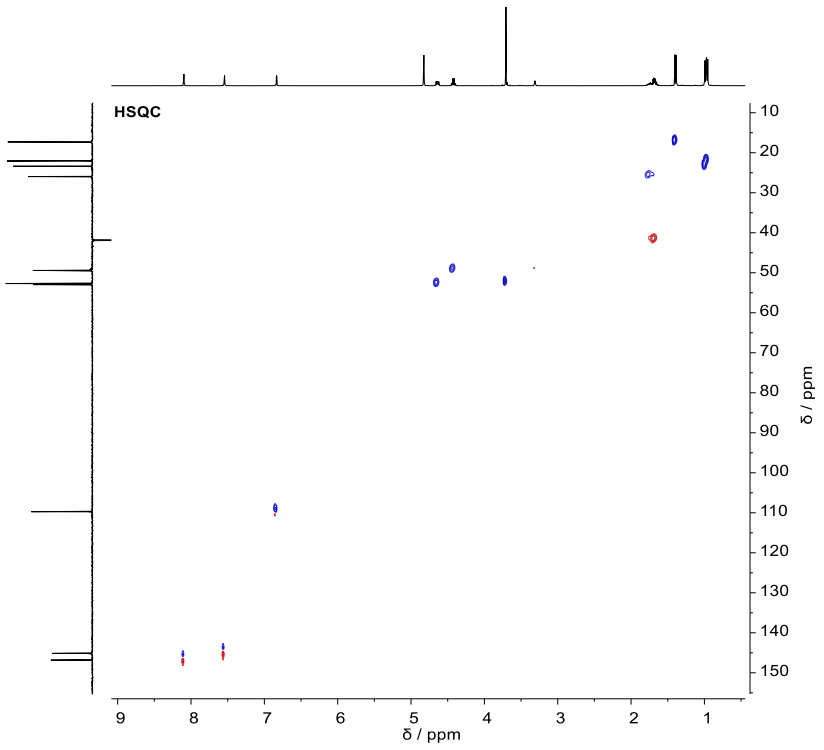

Figure S20. HSQC spectrum (CD_3OD, 400 MHz) of **5a**.

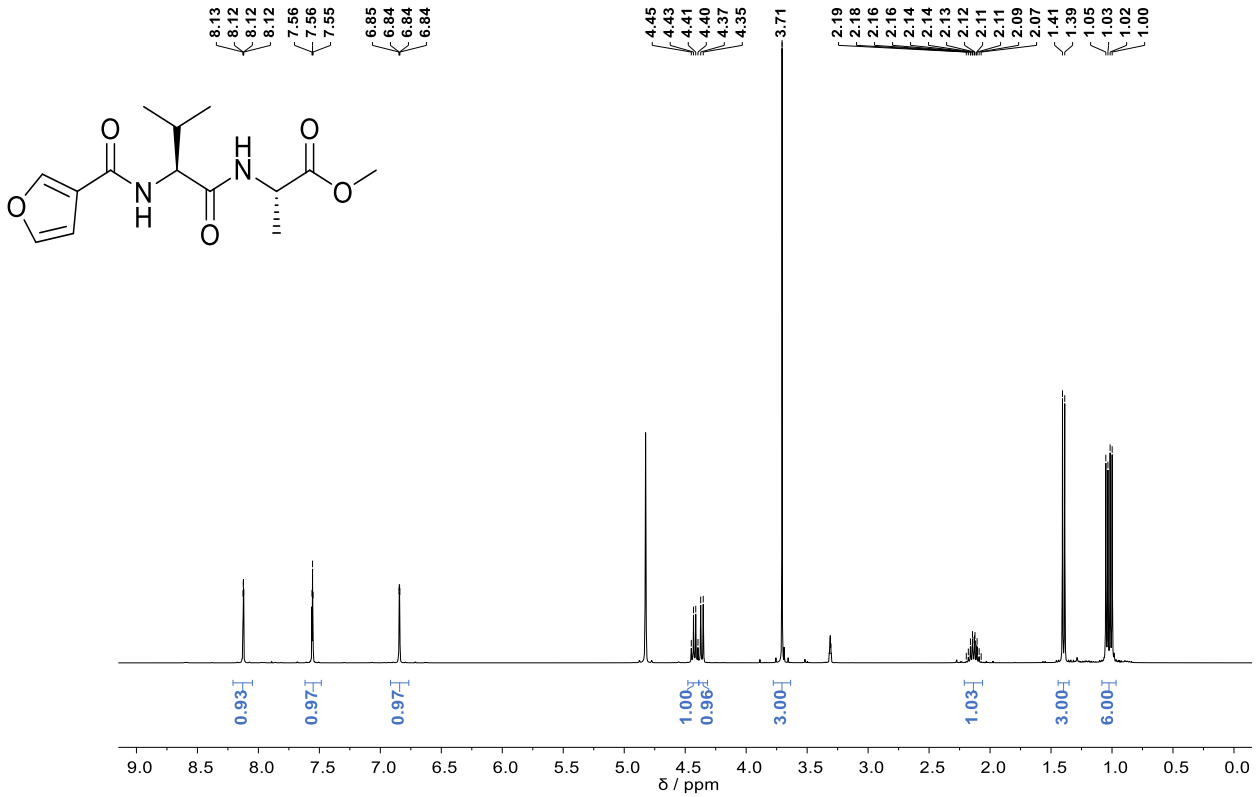

Figure S21. ^{1}H NMR spectrum (CD_3OD, 400 MHz) of **5b**.

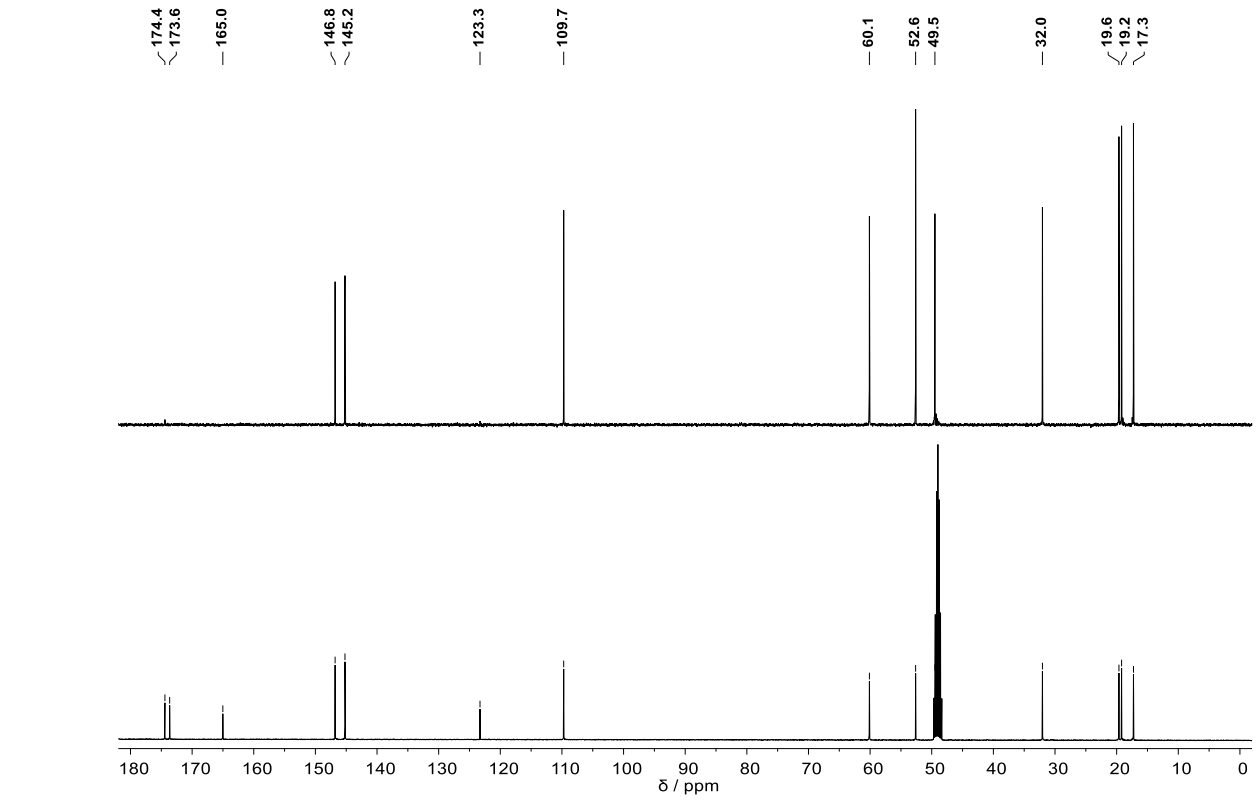

Figure S22. $^{13}C\{^{1}H\}$ NMR and DEPT-135 spectra (CD_3OD, 100 MHz) of **5b**.

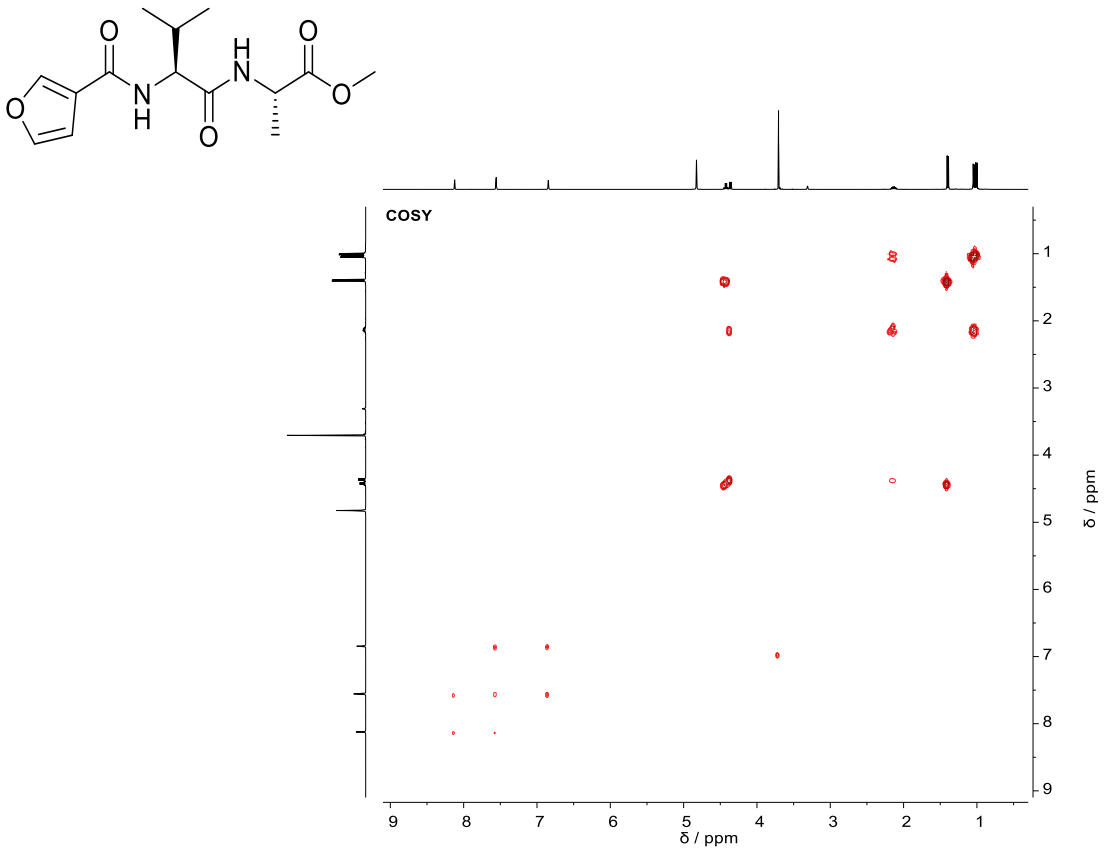

Figure S23. COSY spectrum (CD_3OD, 400 MHz) of **5b**.

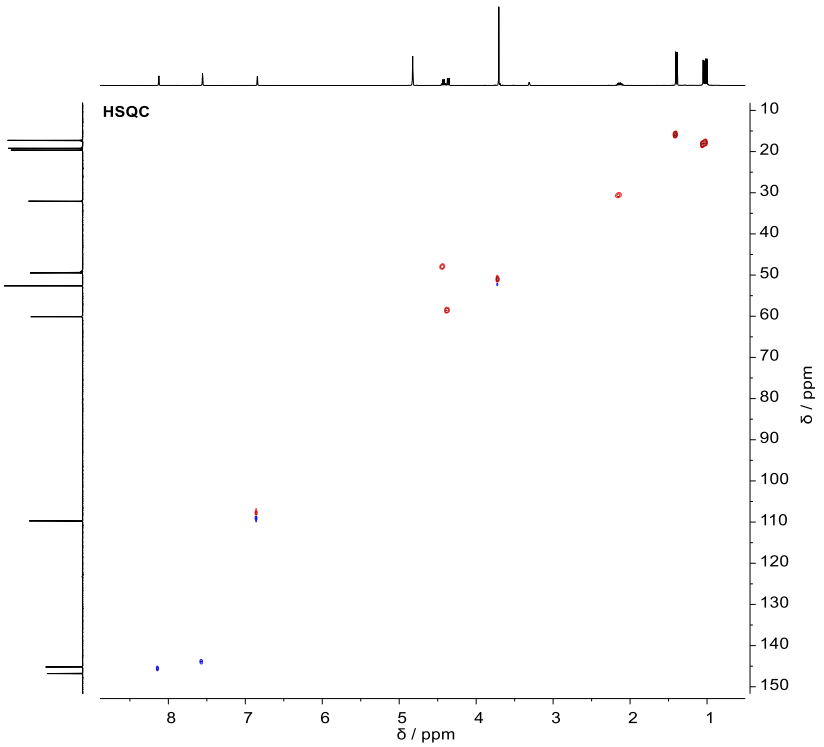

Figure S24. HSQC spectrum (CD_3OD, 400 MHz) of **5b**.

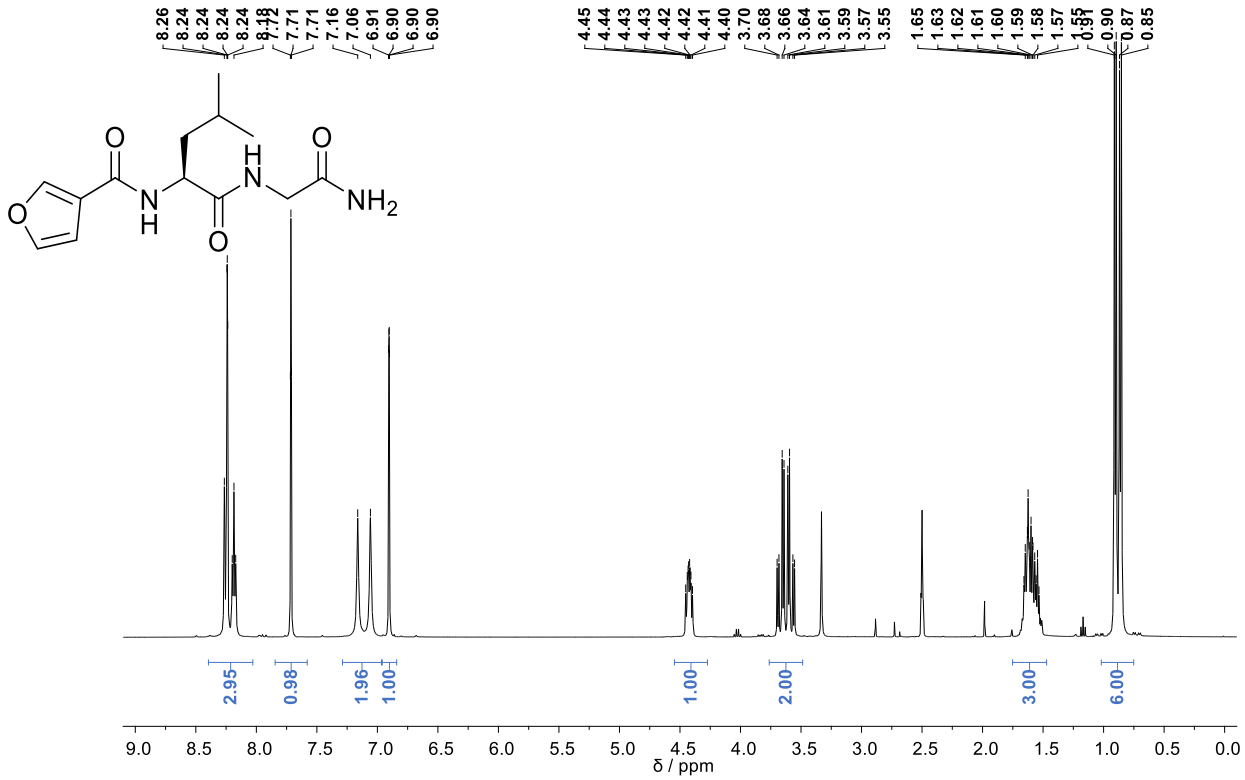

Figure S25. ^{1}H NMR spectrum (DMSO-d_6, 400 MHz) of **6a**.

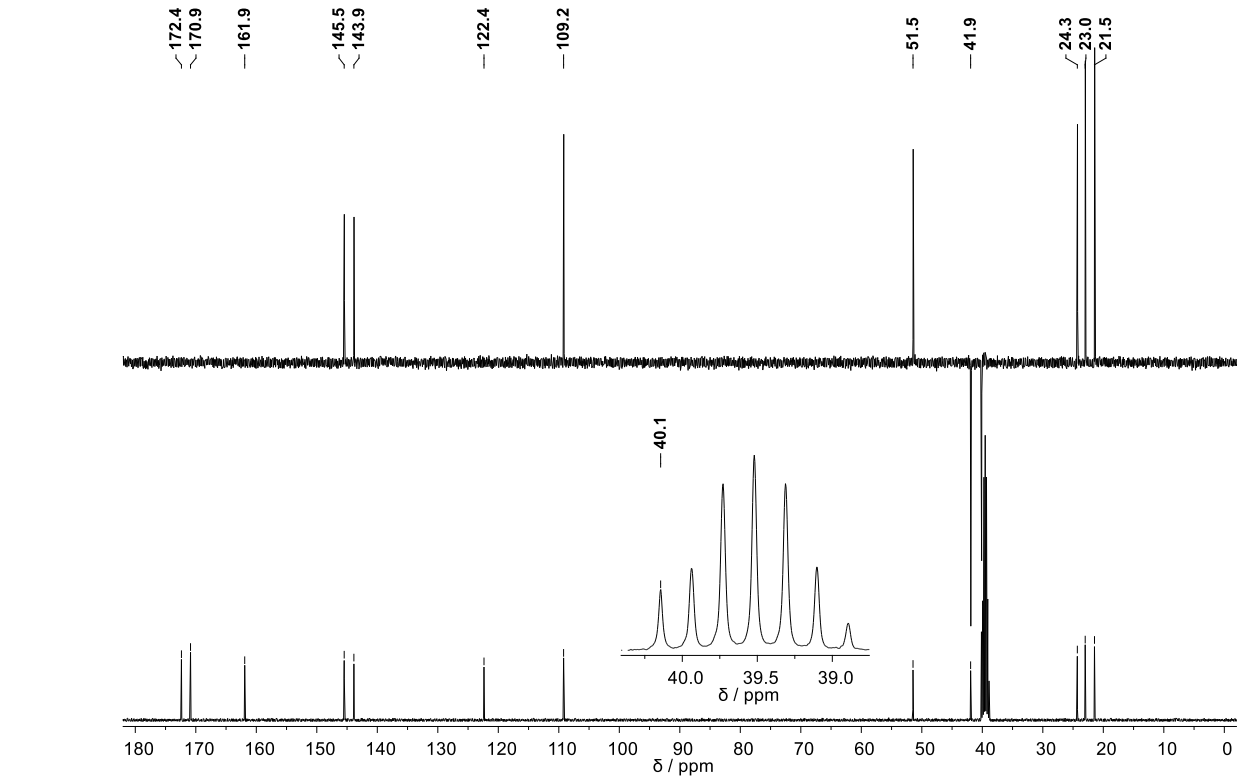

Figure S26. ^{13}C{^{1}H} NMR and DEPT-135 spectra (DMSO-d_6, 100 MHz) of **6a**.

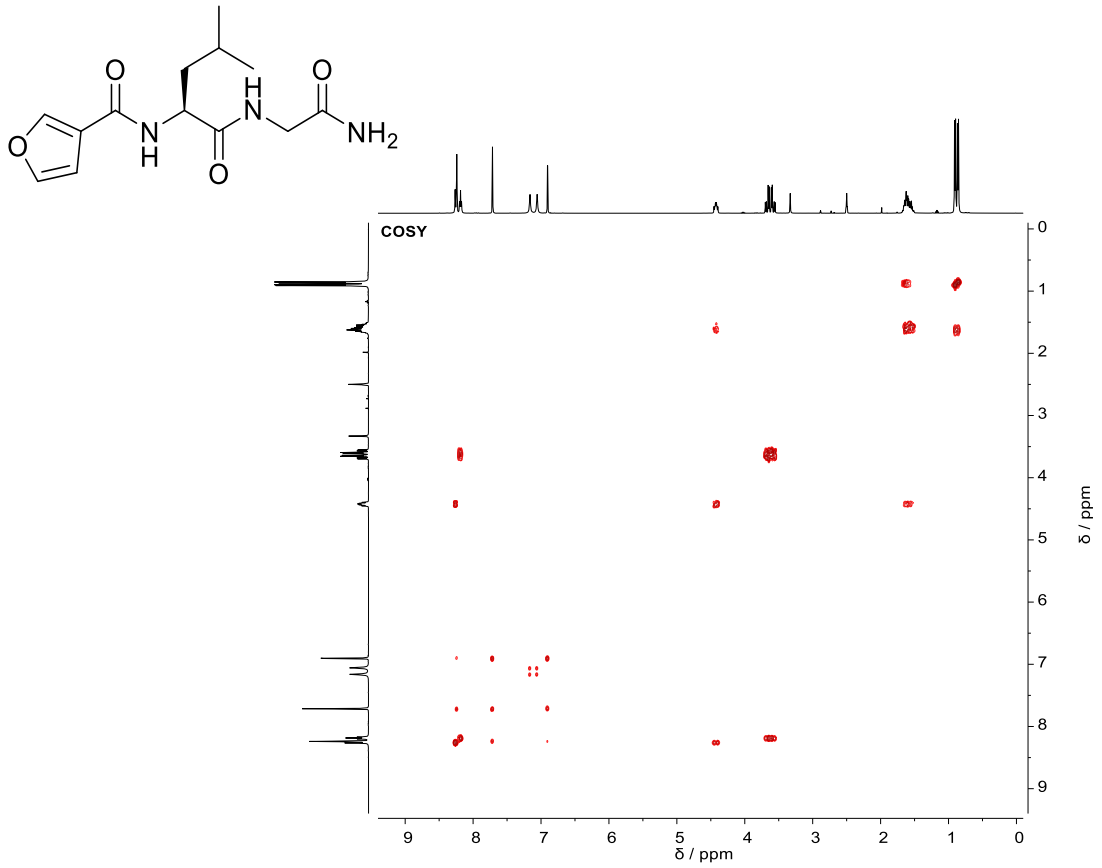

Figure S27. COSY spectrum (DMSO-d_6, 400 MHz) of **6a**.

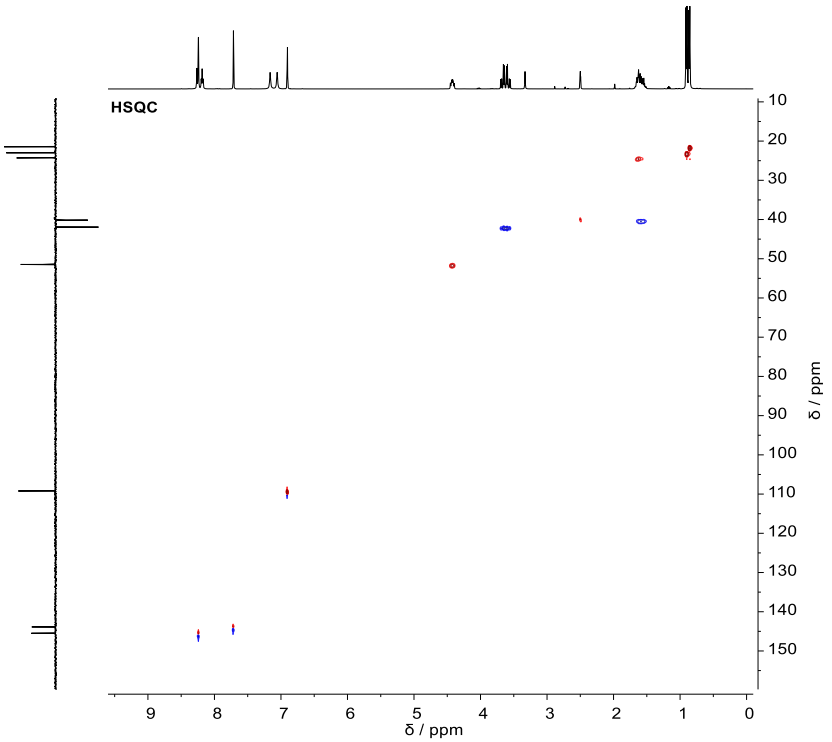

Figure S28. HSQC spectrum (DMSO-d_6, 400 MHz) of **6a**.

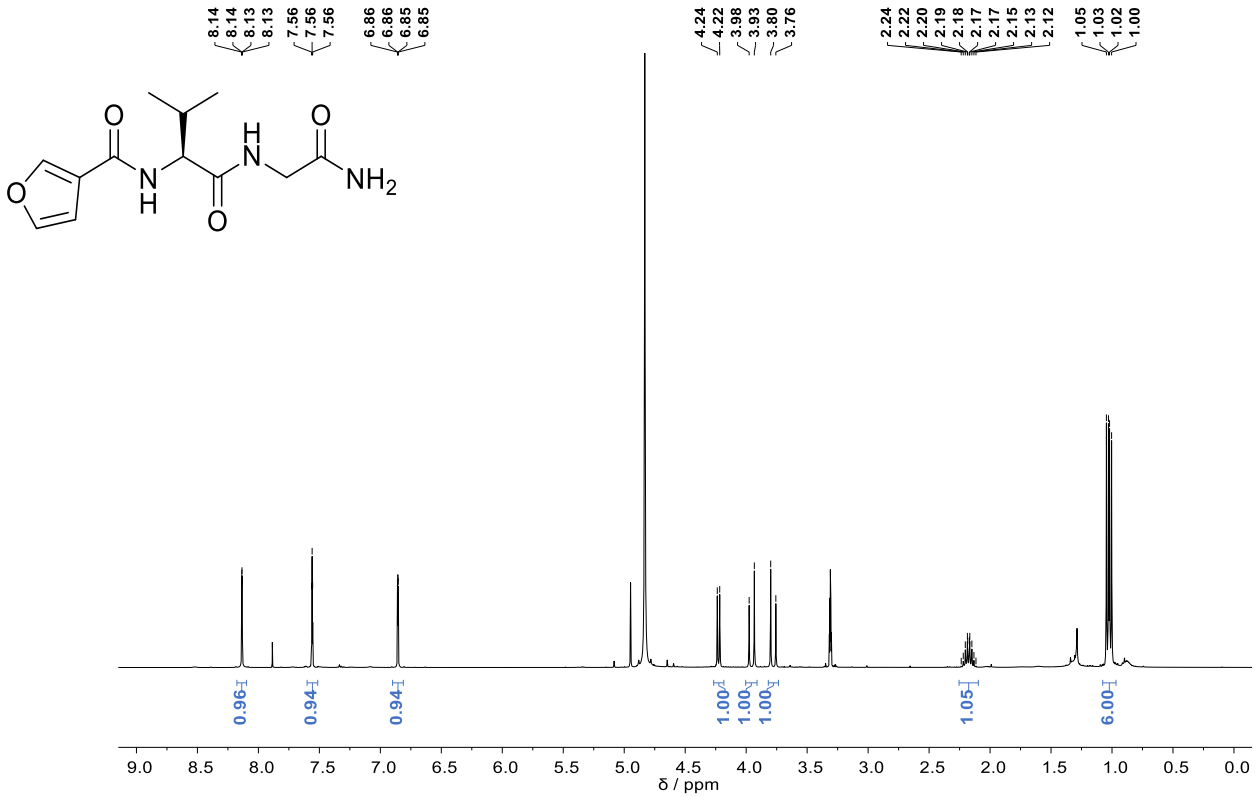

Figure S29. ^{1}H NMR spectrum (CD_3OD, 400 MHz) of **6b**.

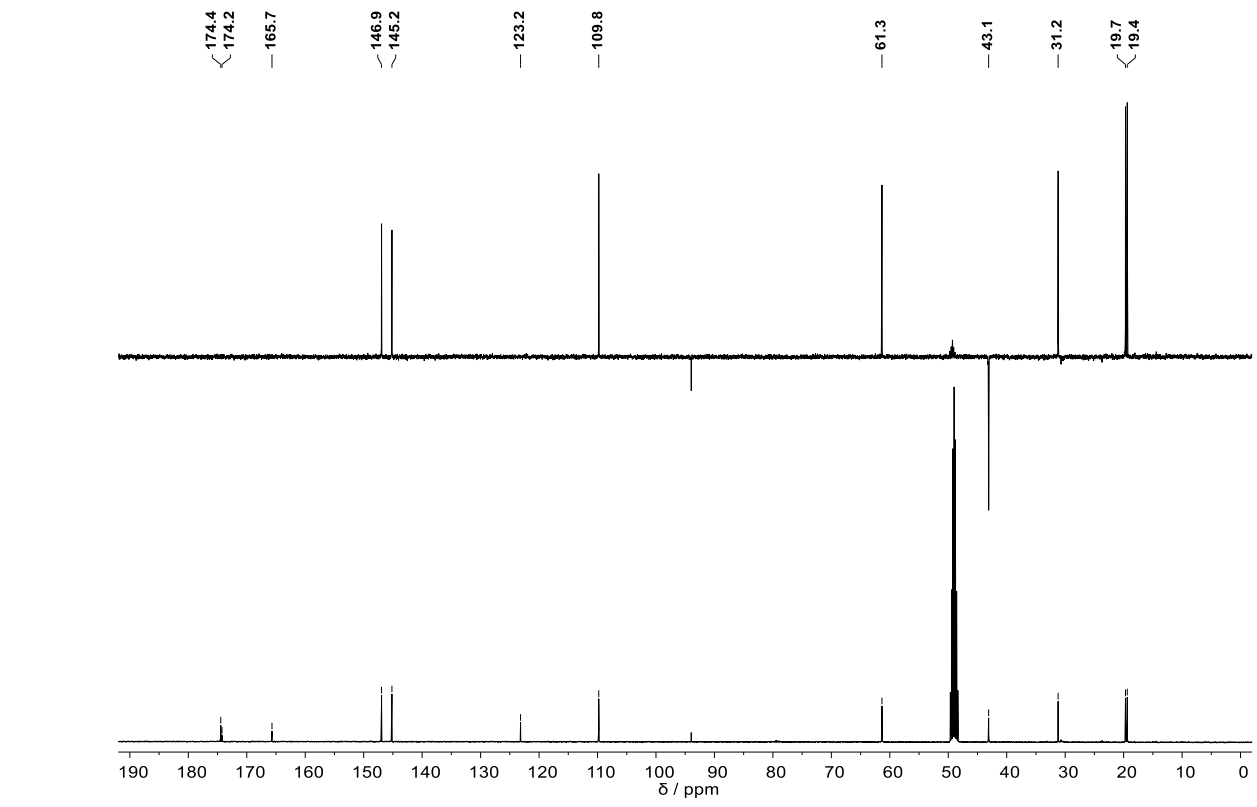

Figure S30. $^{13}C\{^{1}H\}$ NMR and DEPT-135 spectra (CD_3OD, 100 MHz) of **6b**.

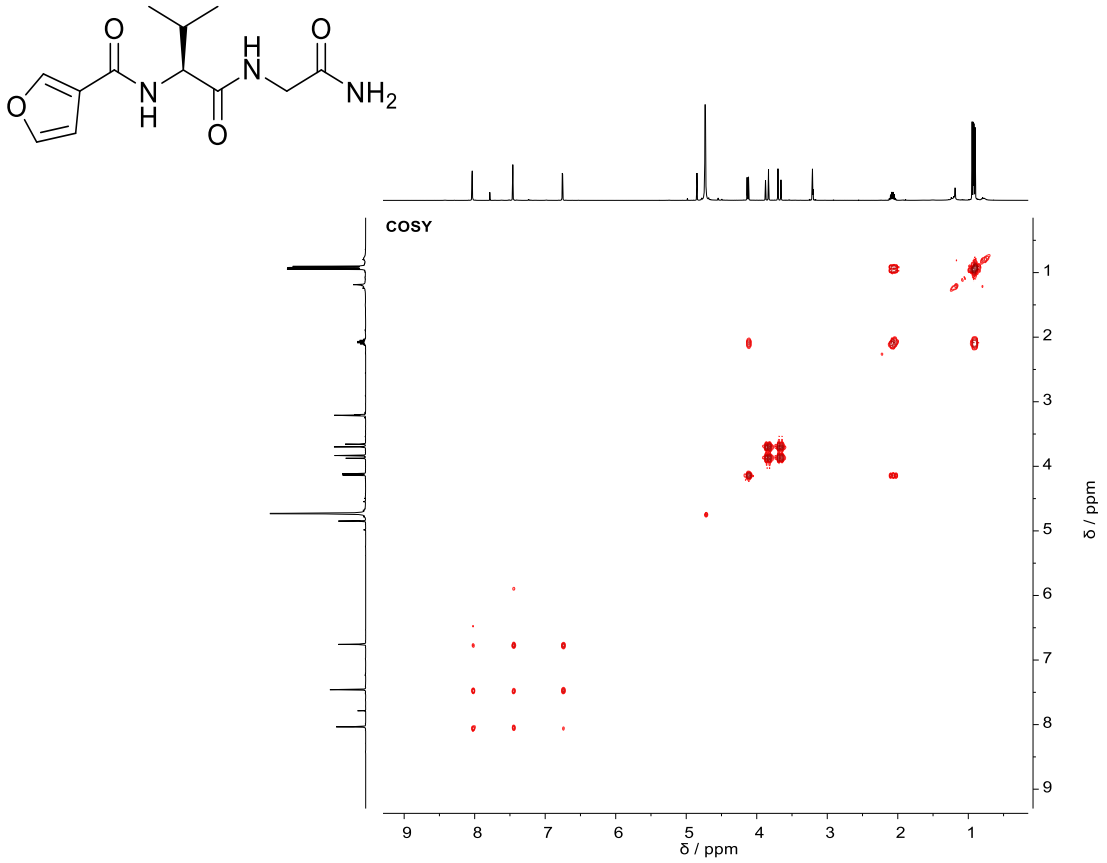

Figure S31. COSY spectrum (CD_3OD, 400 MHz) of **6b**.

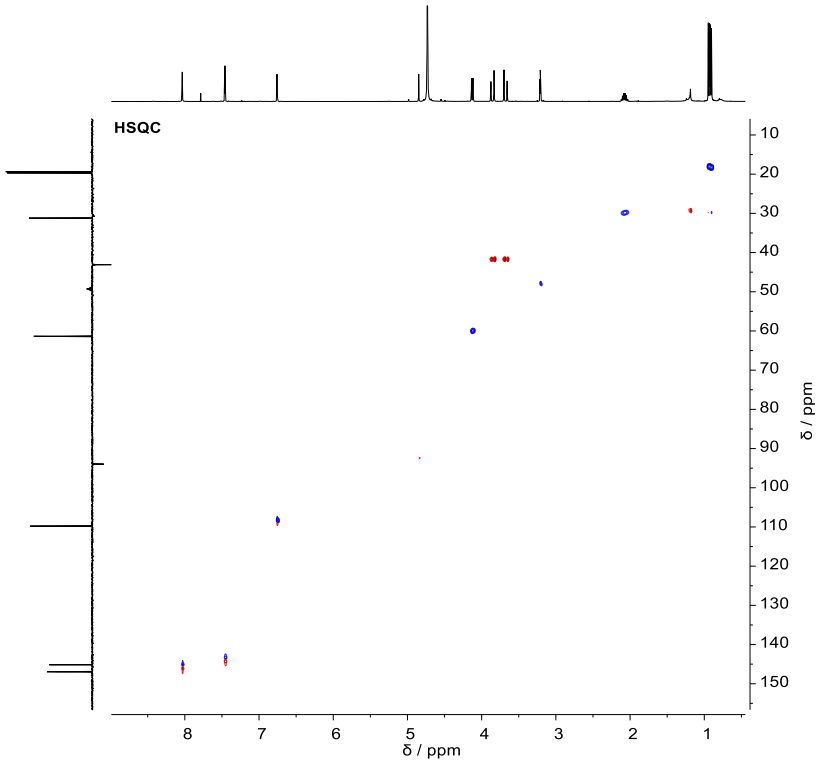

Figure S32. HSQC spectrum (CD_3OD, 400 MHz) of **6b**.

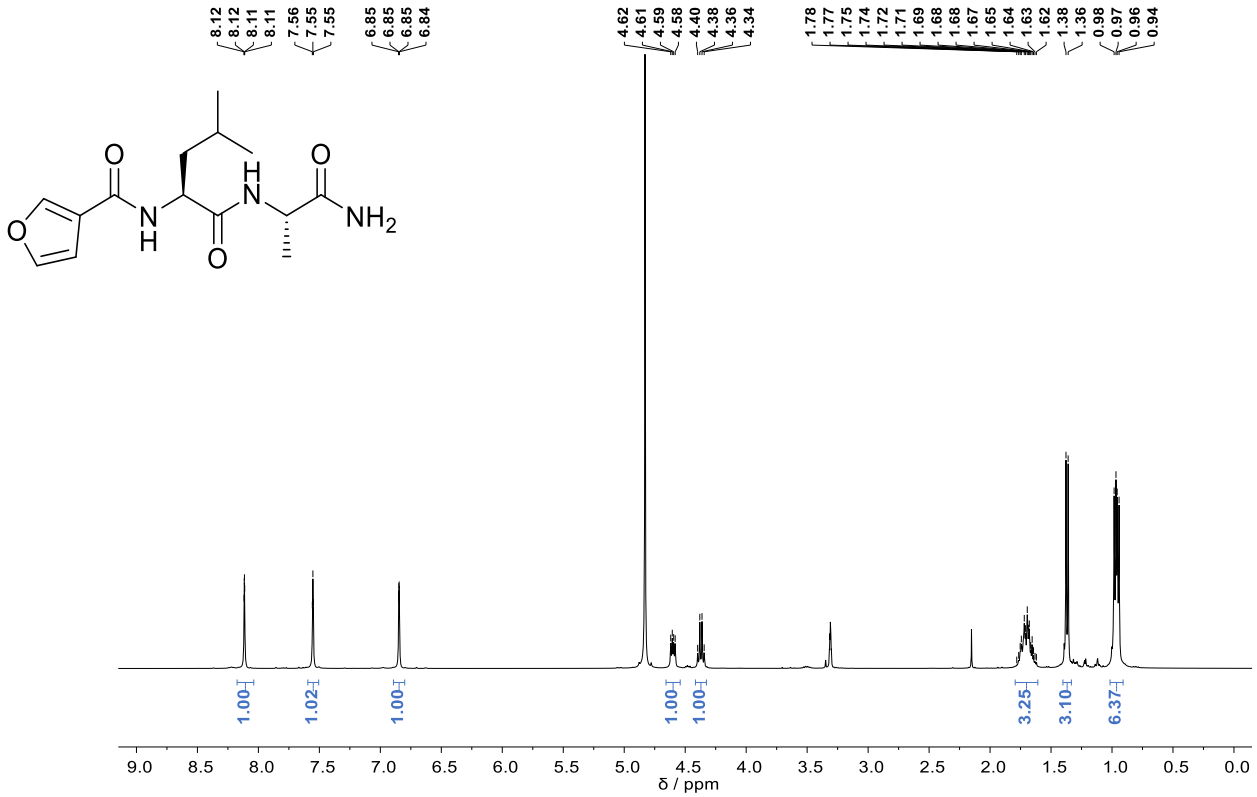

Figure S33. ^{1}H NMR spectrum (CD_3OD, 400 MHz) of **7a**.

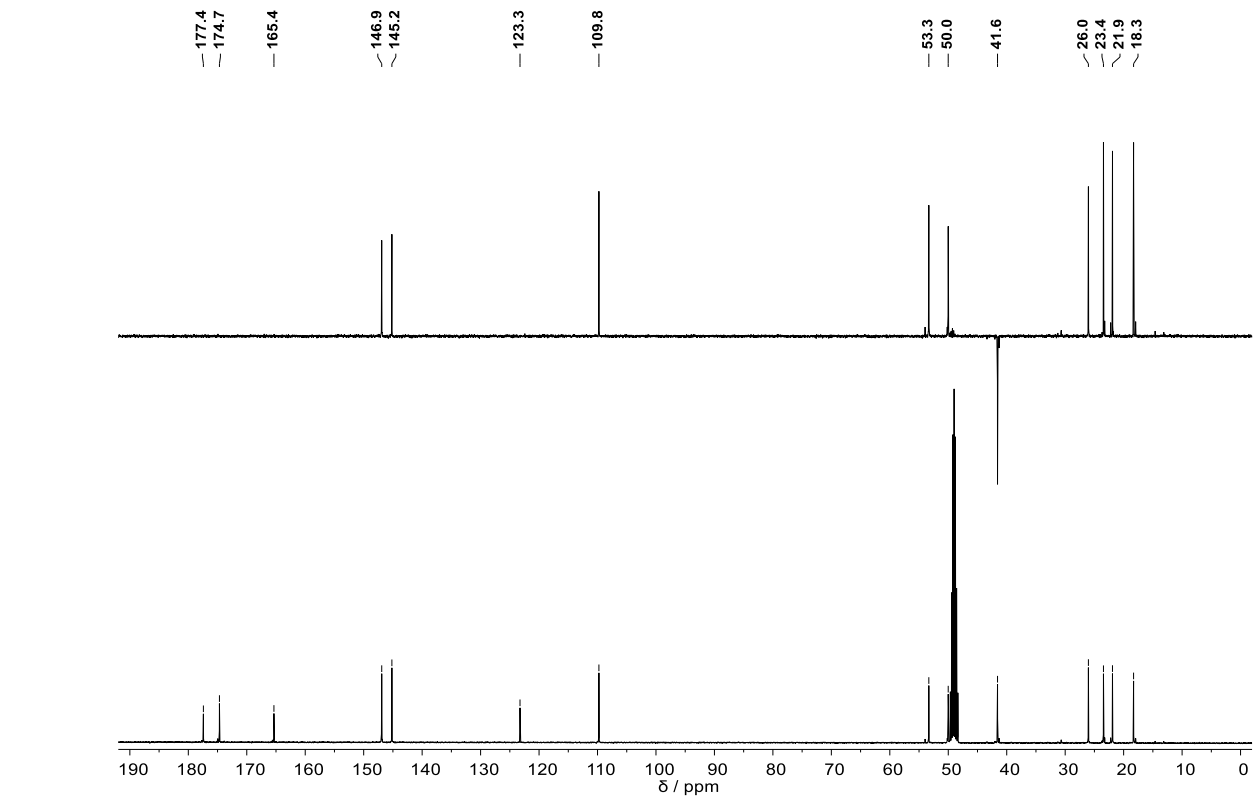

Figure S34. $^{13}C\{^{1}H\}$ NMR and DEPT-135 spectra (CD_3OD, 100 MHz) of **7a**.

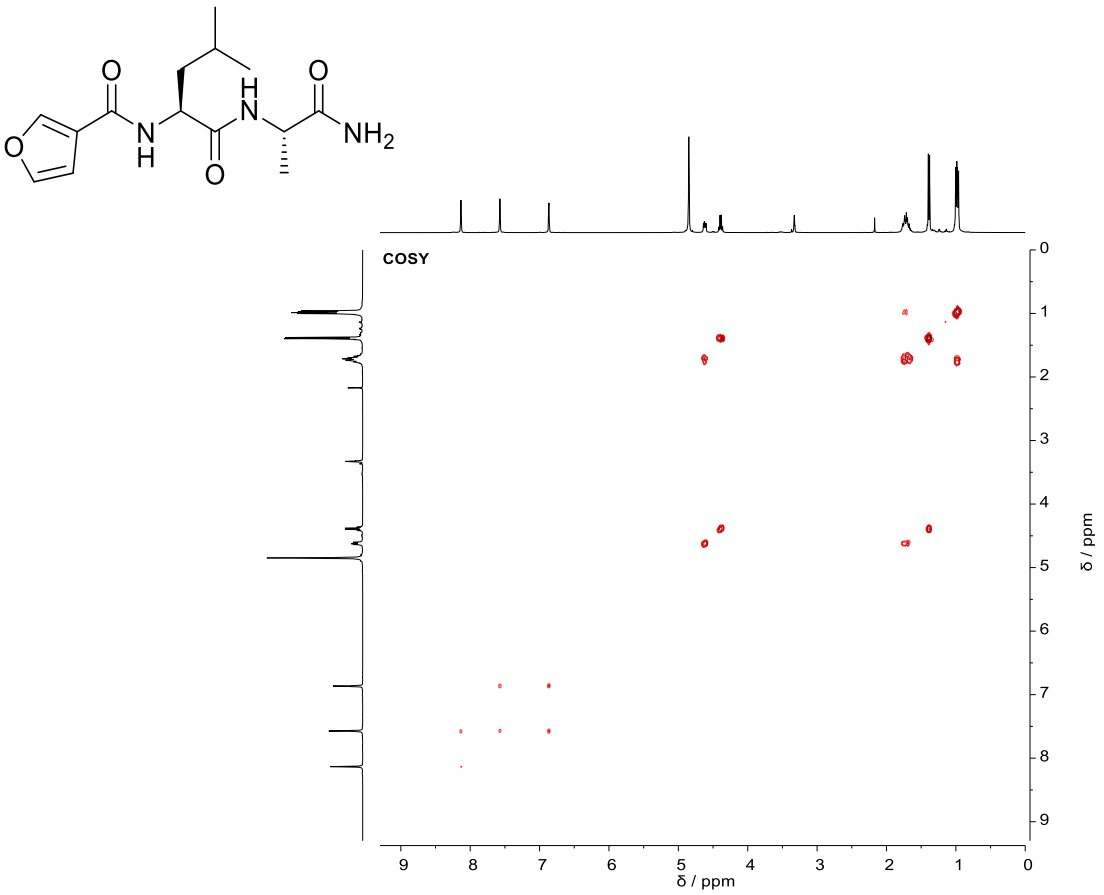

Figure S35. COSY spectrum (CD_3OD, 400 MHz) of **7a**.

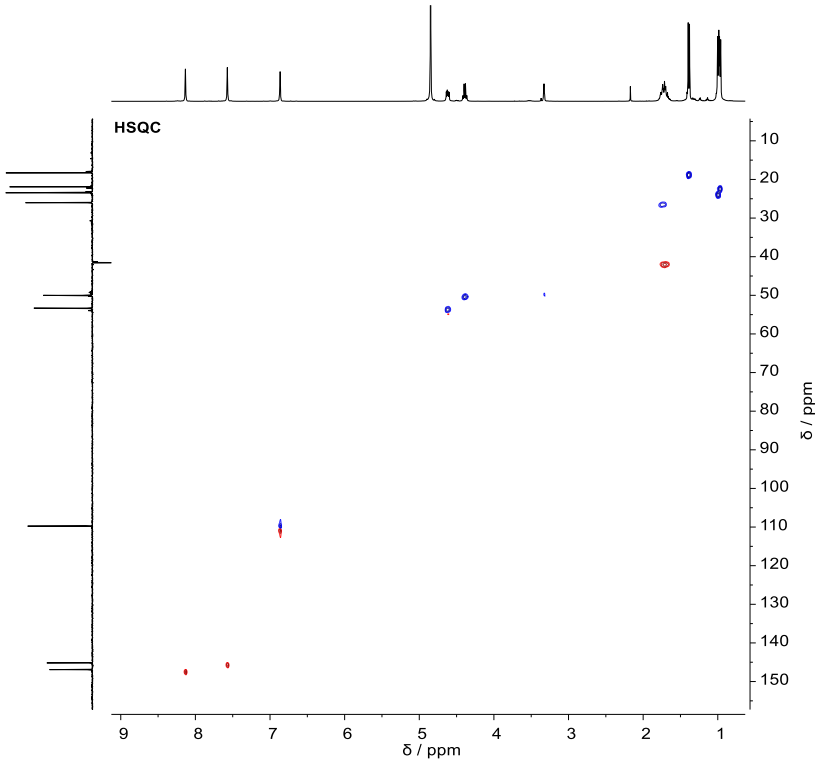

Figure S36. HSQC spectrum (CD_3OD, 400 MHz) of **7a**.

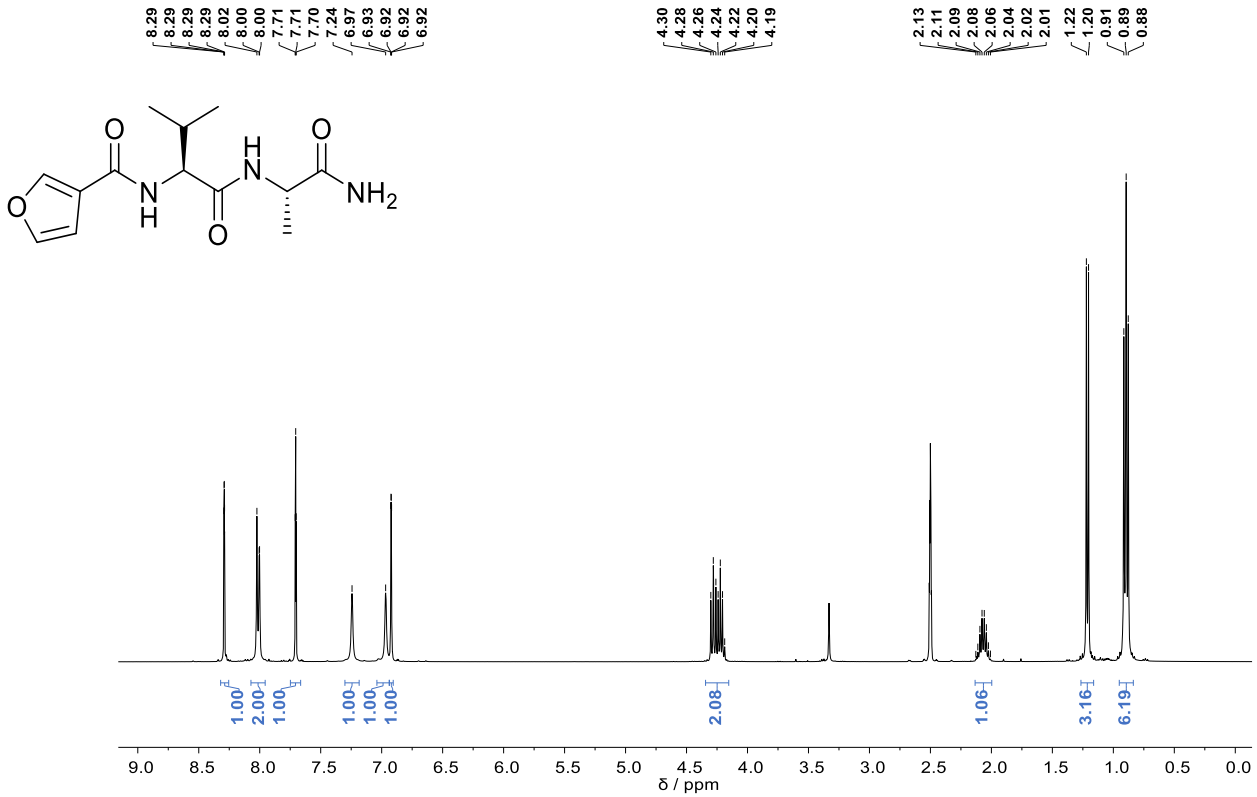

Figure S37. ^{1}H NMR spectrum (DMSO-d_6, 400 MHz) of **7b**.

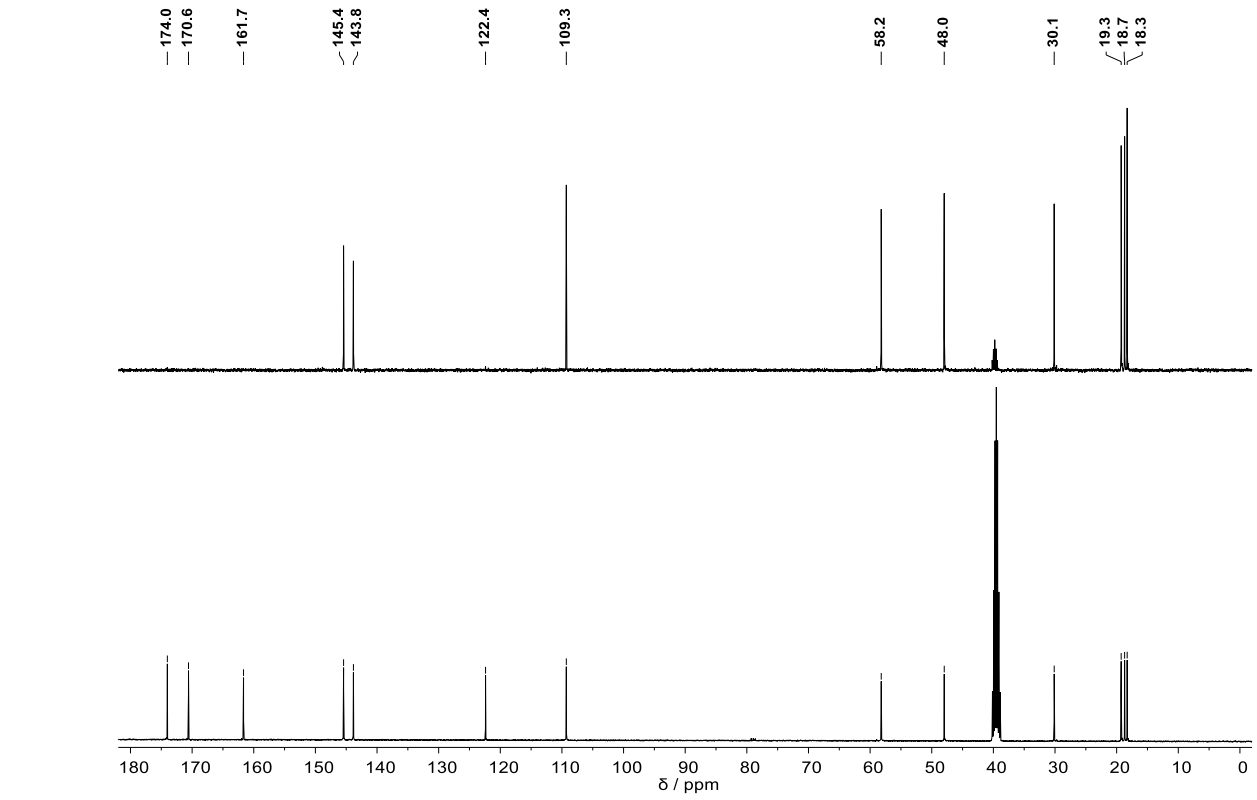

Figure S38. ^{13}C{^{1}H} NMR and DEPT-135 spectra (DMSO-d_6, 100 MHz) of **7b**.

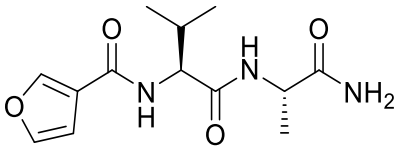

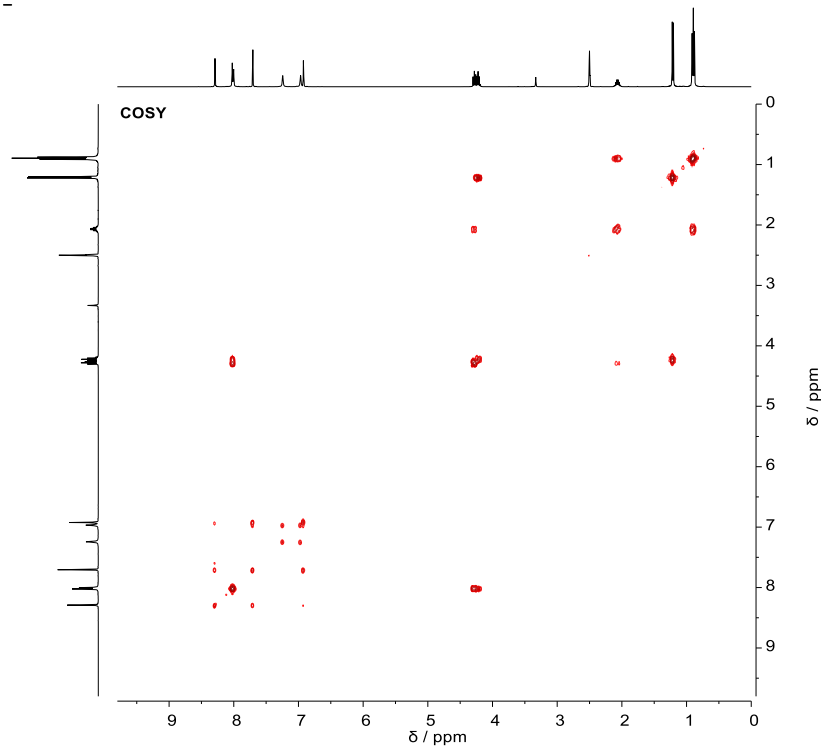

Figure S39. COSY spectrum (DMSO-d_6, 400 MHz) of **7b**.

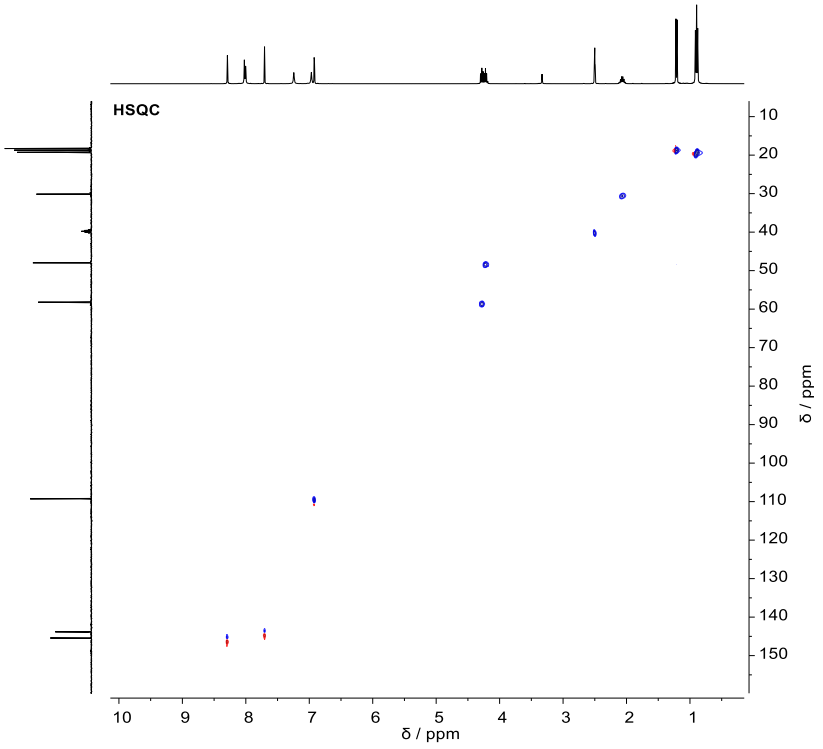

Figure S40. HSQC spectrum (DMSO-d_6, 400 MHz) of **7b**.

2. RP-HPLC chromatograms

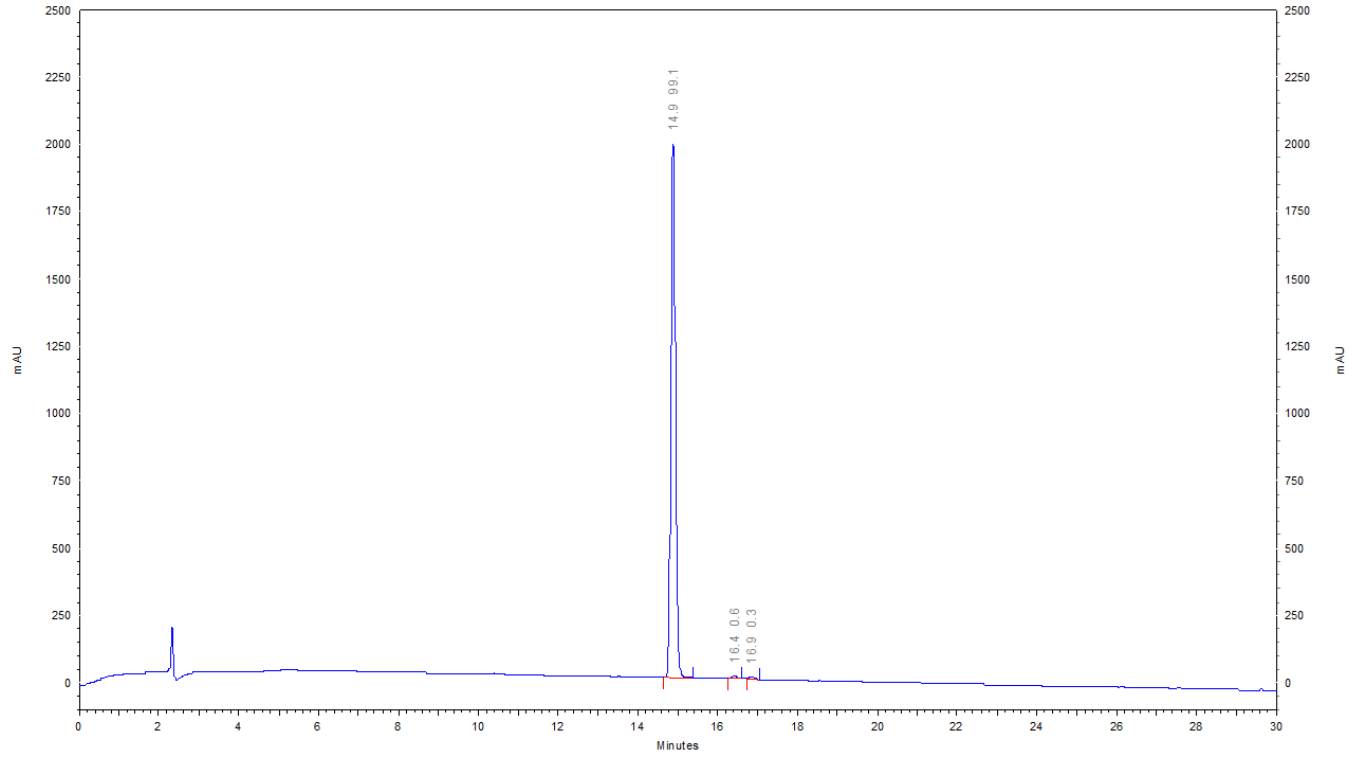

Figure S41. HPLC chromatogram of **4a**. R_t = 14.9 min, % area = 99.1%.

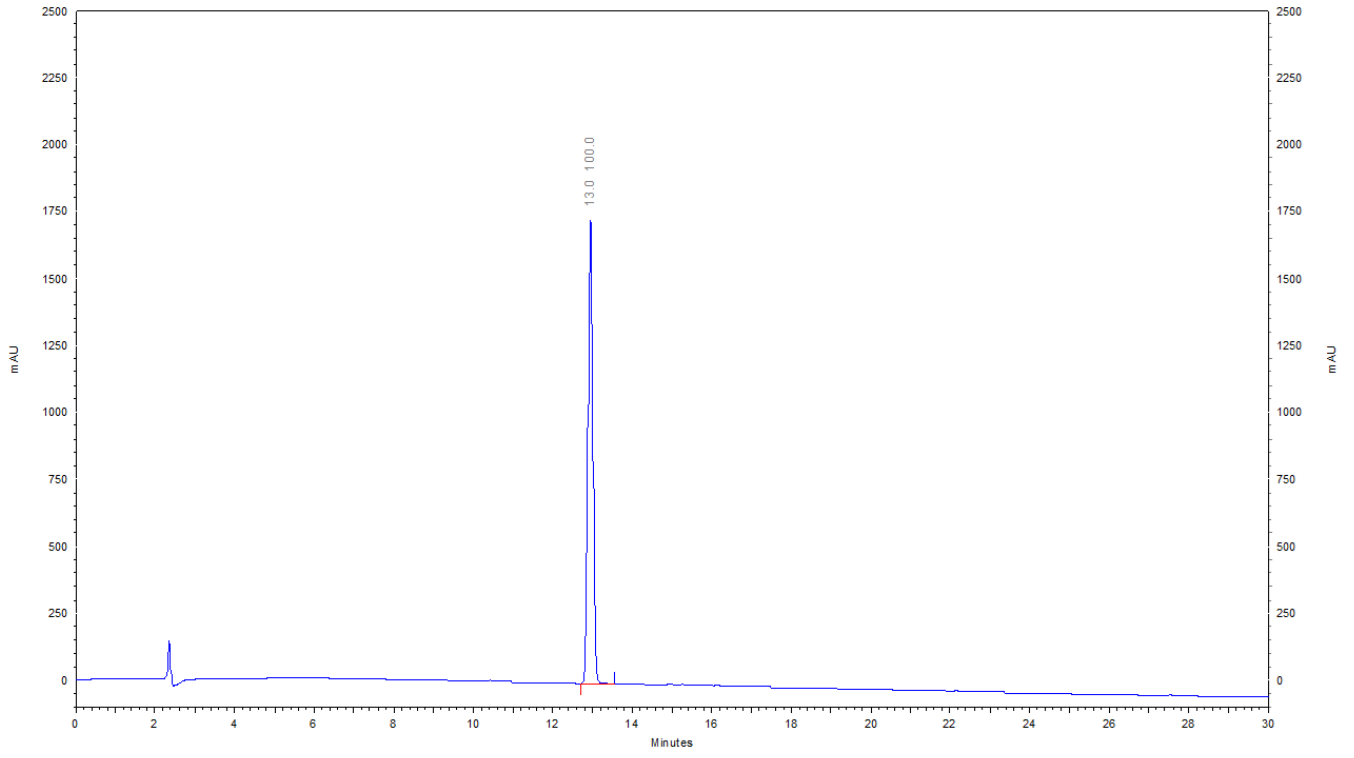

Figure S42. HPLC chromatogram of **4b**. R_t = 13.0 min, % area = 100%.

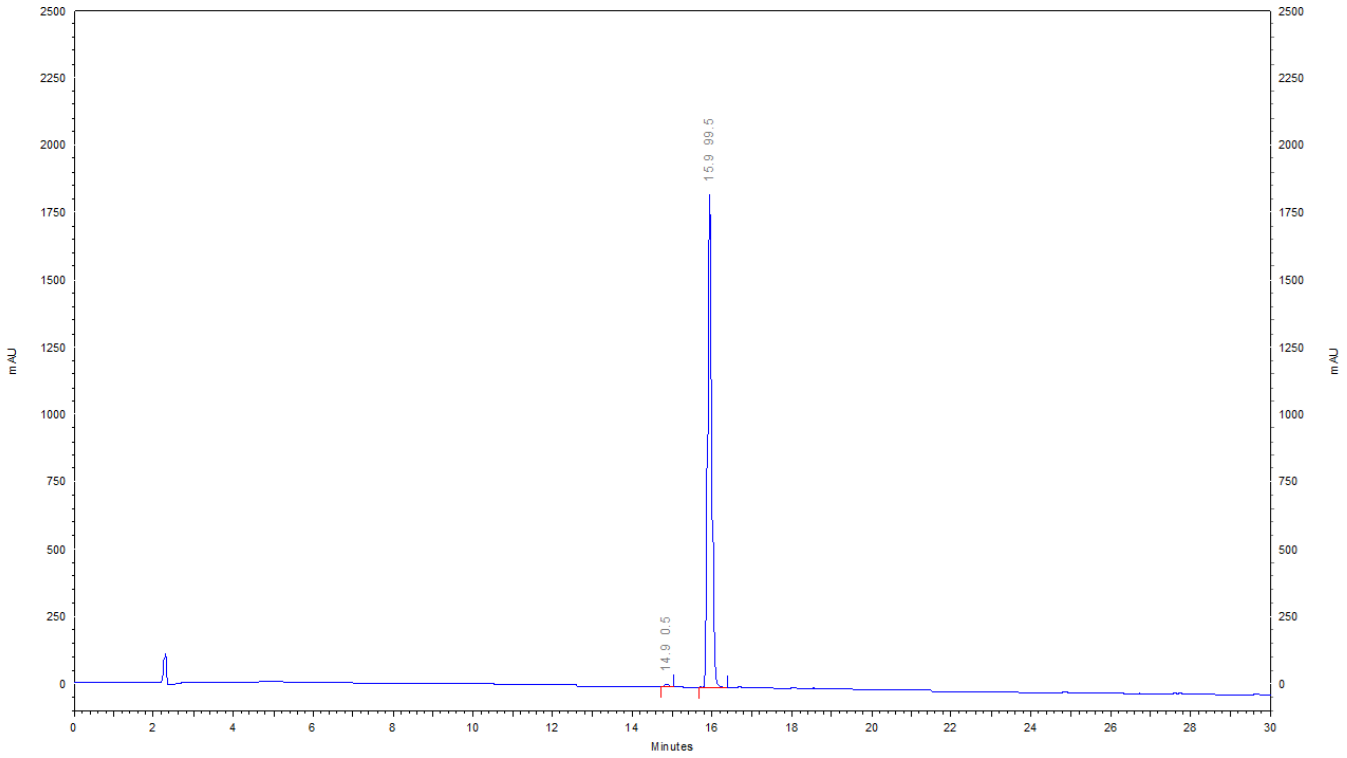

Figure S43. HPLC chromatogram of **5a**. R_t = 15.9 min, % area = 99.5%.

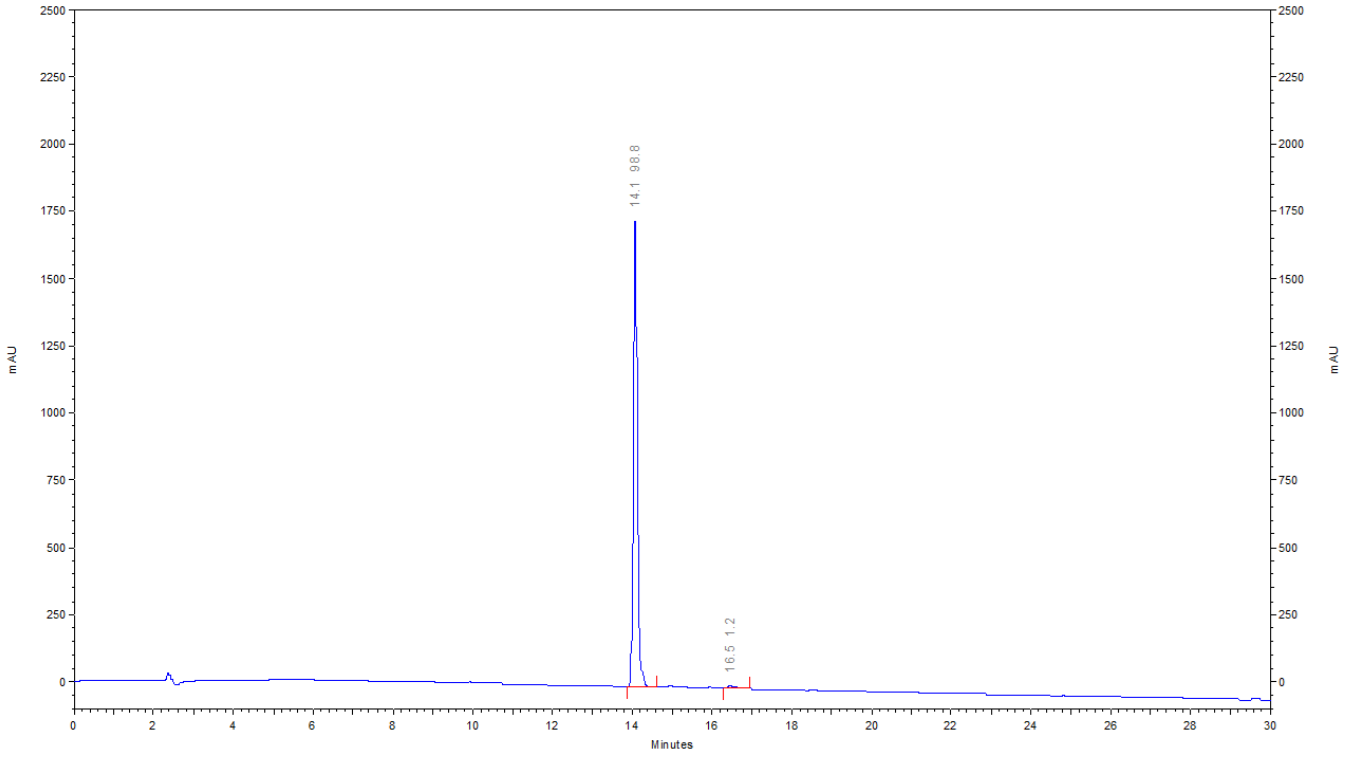

Figure S44. HPLC chromatogram of **5b**. R_t = 14.1 min, % area = 98.8%.

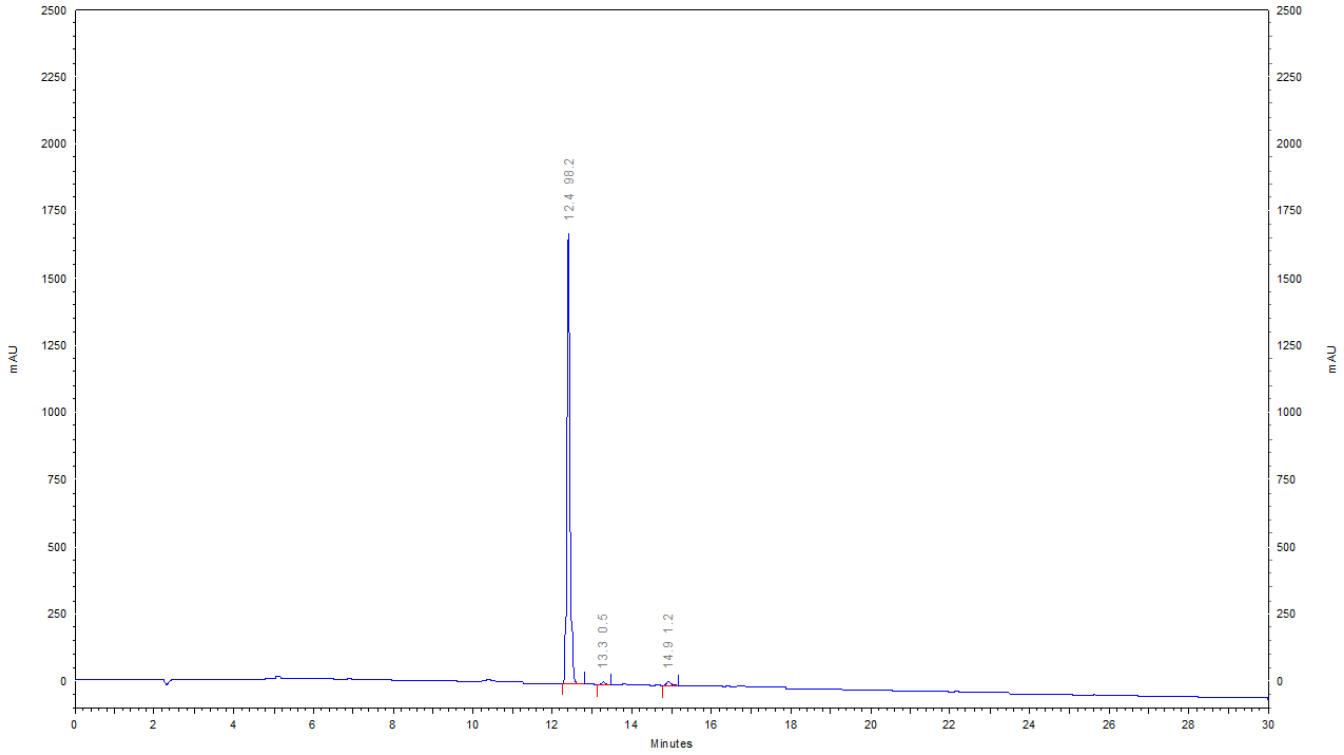

Figure S45. HPLC chromatogram of **6a**. R_t = 12.4 min, % area = 98.2%.

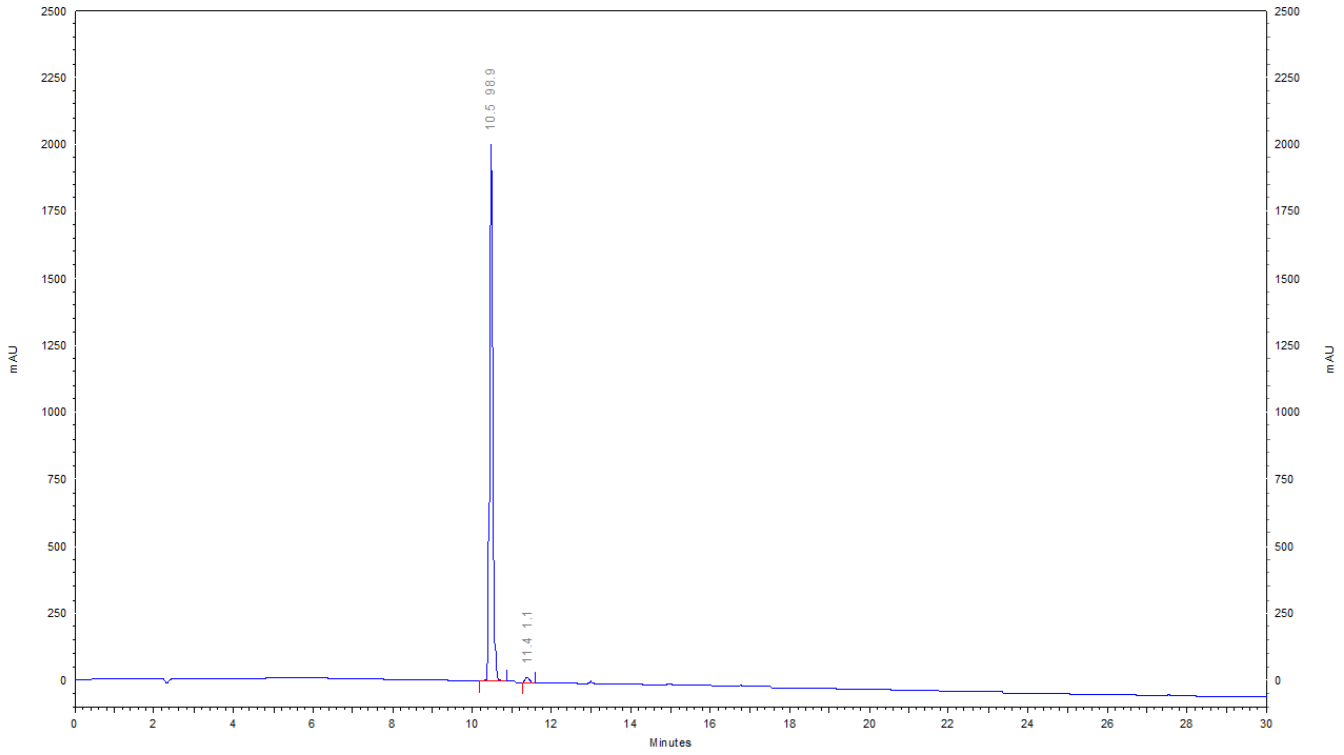

Figure S46. HPLC chromatogram of **6b**. R_t = 10.5 min, % area = 98.9%.

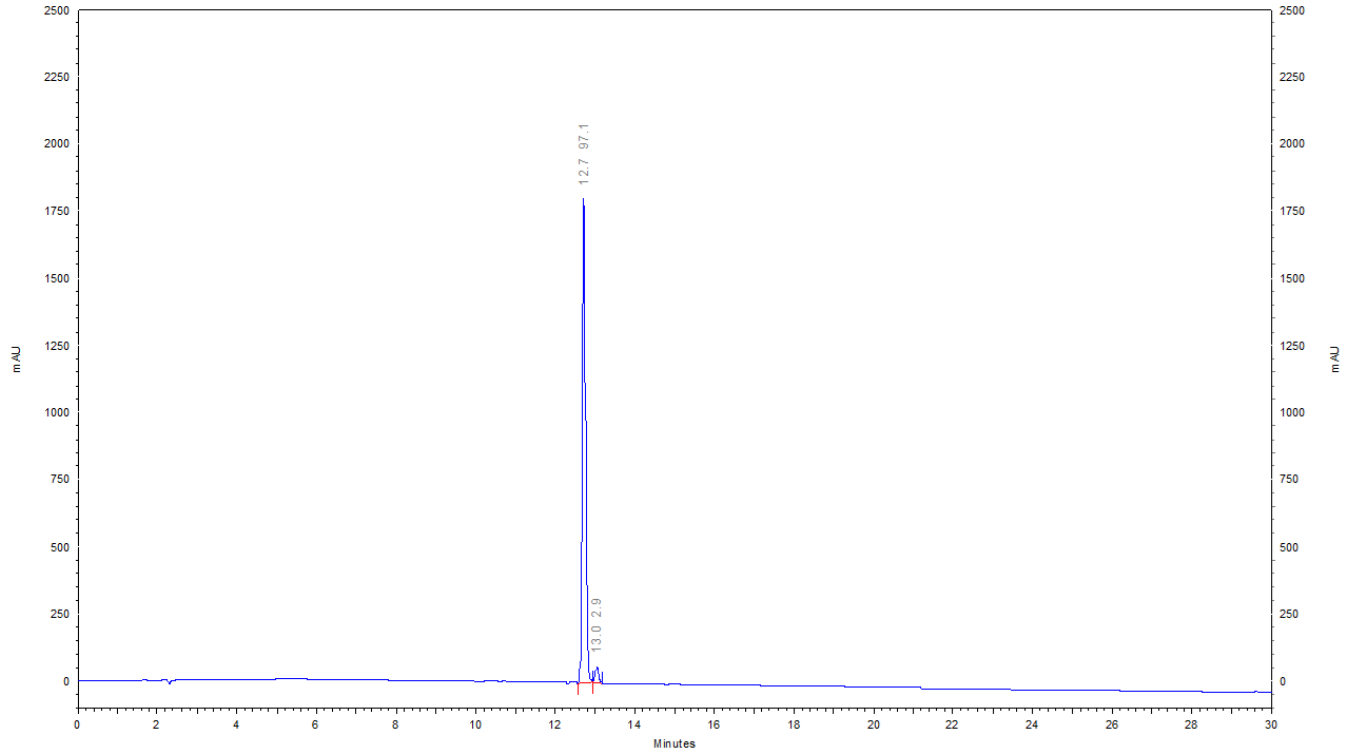

Figure S47. HPLC chromatogram of **7a**. R_t = 12.7 min, % area = 97.1%.

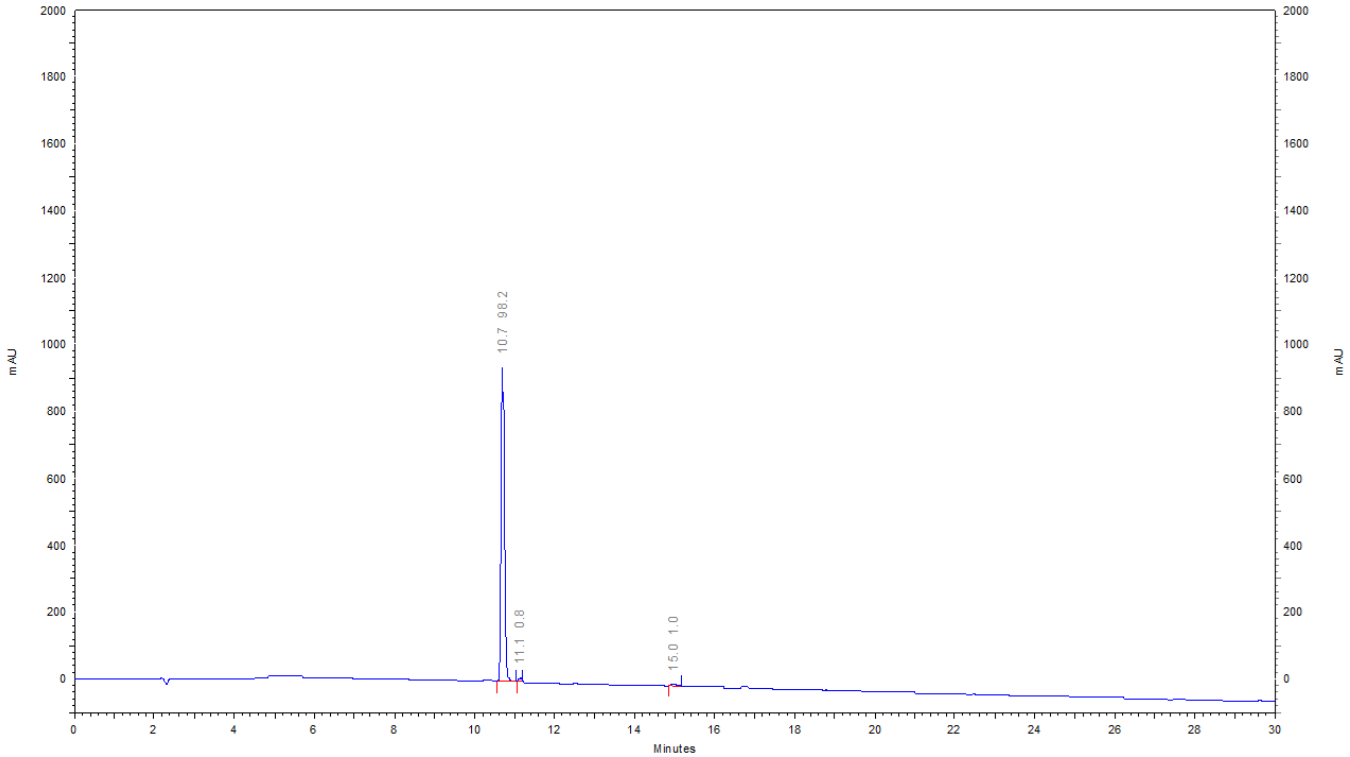

Figure S48. HPLC chromatogram of **7b**. R_t = 10.7 min, % area = 98.2%.

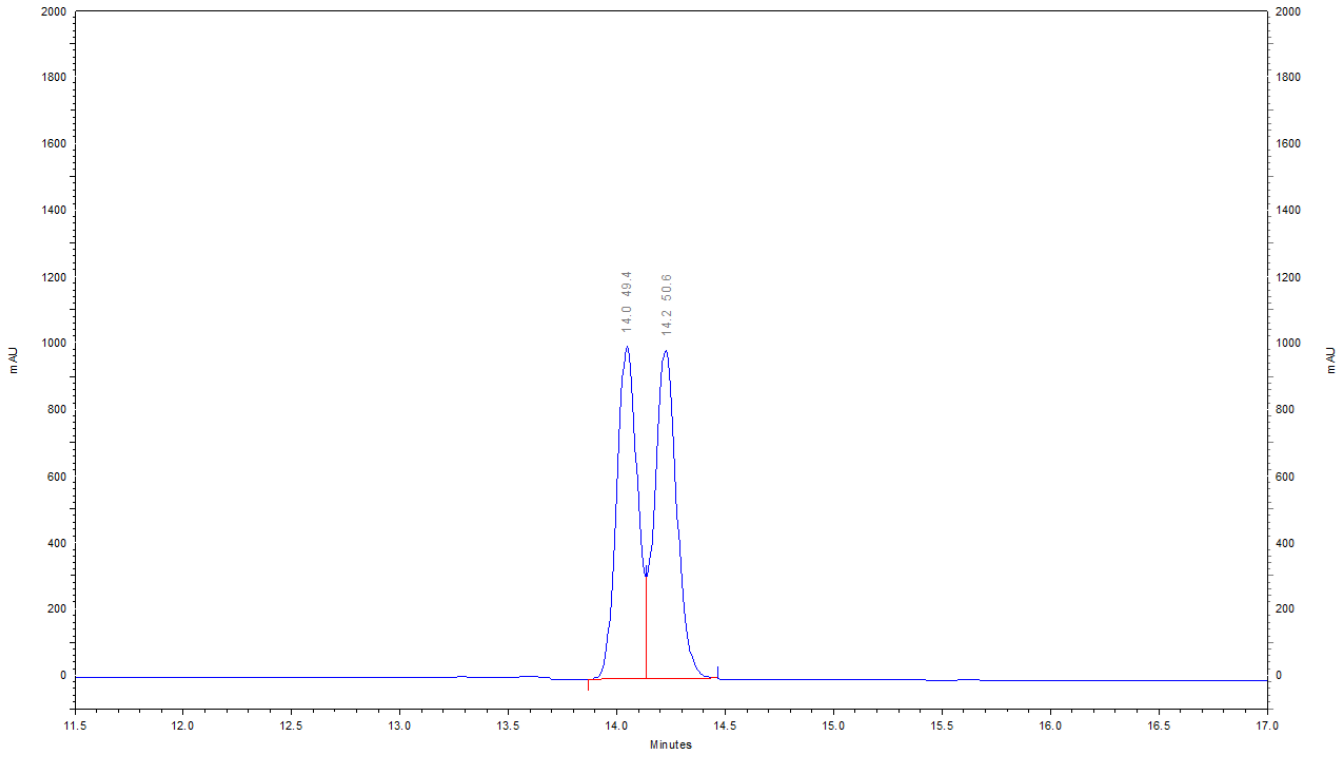

Figure S49. HPLC chromatogram of **5b/5b'**. R_t of **5b** = 14.0 min, % area = 49.4%; R_t of **5b'** = 14.2 min, % area = 50.6%.

3. Functional assays

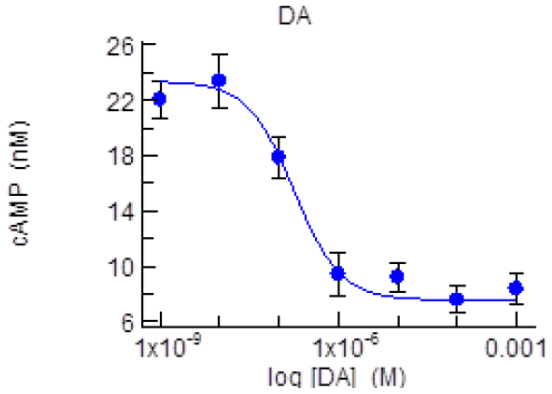

Figure S50. Concentration-response curve of DA at human D_2R. The mean ± SEM (vertical bars) of each measure was determined in duplicate.

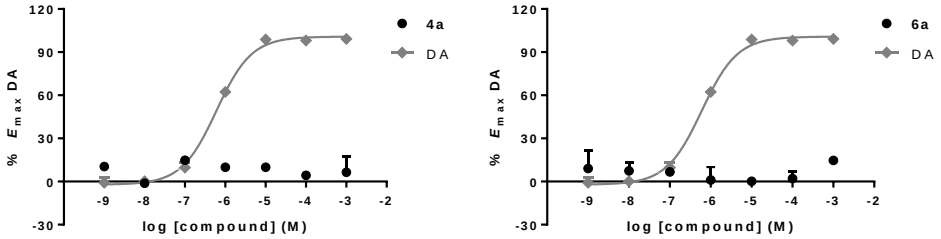

Figure S51. Concentration-response curves of peptidomimetics **4a** and **6a** at human D_2R (including the concentration-response curve of DA for comparison). Data represent the mean ± SD of three independent measurements.

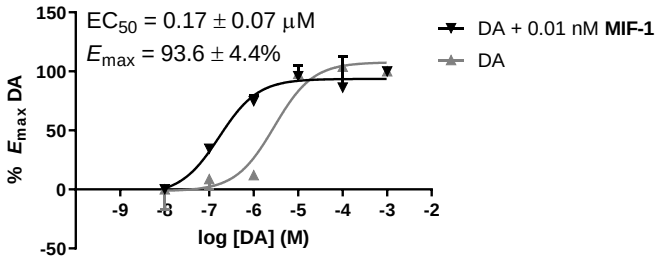

Figure S52. Concentration-response curve of DA in the presence of 0.01 nM of MIF-1 (including the concentration-response curve of DA).[1] Data represent the mean ± SD (vertical bars) of two independent experiments with duplicate measurements.

Table S1. Percentage of increase of DA effect shown by the inactive compounds at 0.01 and 0.1 nM.

Compound	% Effect at 0.01 nM (Mean ± SD)	% Effect at 0.1 nM (Mean ± SD)
I	−65.24 ± 11.12	−98.45 ± 11.97
4b	7.06 ± 9.49	9.31 ± 15.42
5a	4.01 ± 7.54	−31.33 ± 2.26
5b	2.92 ± 12.34	3.77 ± 2.31
6b	−18.74 ± 0.03	−14.82 ± 5.57
7a	3.34 ± 0.82	1.08 ± 0.74
7b	−37.06 ± 15.62	4.54 ± 5.44

4. Tables of cartesian coordinates

Table S2. Cartesian coordinates of **4a**, at the M06-2X level of theory, with zero imaginary frequencies and a total energy of −1030.83809828 hartree.

Atom	Cartesian coordinates		
	x	*y*	*z*
O	-12.00261	0.08139	1.05445
C	-12.12415	0.20791	-0.30505
C	-10.81593	0.62316	1.40751
C	-10.16942	1.09529	0.30392
C	-11.03181	0.82136	-0.81788
C	-8.84553	1.74695	0.36094
N	-8.27527	2.03897	-0.82270
O	-8.30013	1.98404	1.45518
C	-7.06011	2.82815	-1.03928
C	-5.76223	2.08245	-0.72222
C	-7.10024	4.19368	-0.33189
C	-5.91215	5.10779	-0.66015
C	-6.03477	6.39688	0.15229
C	-5.82115	5.42831	-2.15277
O	-4.81252	2.12377	-1.51740
N	-5.68619	1.42244	0.44463
C	-4.46237	0.77246	0.83414
C	-3.34961	1.75901	1.12792
O	-3.48602	2.96050	1.24098
O	-2.18452	1.12965	1.26920
C	-1.04995	1.95364	1.59326
H	-13.03423	-0.18085	-0.73557
H	-10.56413	0.60310	2.45750
H	-10.86718	1.05234	-1.86126
H	-8.77612	1.77250	-1.66112
H	-7.15230	4.04169	0.75011
H	-8.02989	4.68941	-0.64075
H	-4.98608	4.60167	-0.35382
H	-5.18526	7.05999	-0.03975
H	-6.06999	6.18945	1.22685
H	-6.95046	6.93632	-0.11927
H	-6.76068	5.87300	-2.50432
H	-5.61688	4.54084	-2.75943
H	-5.01771	6.14804	-2.34079
H	-6.45736	1.50676	1.10366
H	-4.11732	0.08702	0.05539
H	-4.64039	0.18886	1.74016
H	-0.21010	1.26826	1.68501
H	-1.22420	2.47366	2.53684
H	-0.87157	2.67259	0.79195
H	-7.02687	2.99176	-2.11708

Table S3. Cartesian coordinates of **6a**, at the M06-2X level of theory, with zero imaginary frequencies and a total energy of −971.70097388 hartree.

Atom	Cartesian coordinates		
	x	*y*	*z*
O	-10.67352	-1.54381	0.19783
C	-10.59834	-1.63697	-1.16772
C	-9.56332	-0.90006	0.62211
C	-8.77533	-0.57495	-0.44149
C	-9.45895	-1.05831	-1.61429
C	-7.49236	0.14453	-0.30887
N	-6.83047	0.39189	-1.45447
O	-7.06365	0.47862	0.81110
C	-5.61860	1.20145	-1.60738
C	-4.34658	0.47743	-1.16113
C	-5.73482	2.58926	-0.95805
C	-4.53254	3.50639	-1.21778
C	-4.74763	4.82610	-0.47652
C	-4.31089	3.76648	-2.70835
O	-3.36525	0.40919	-1.91674
N	-4.32920	-0.04693	0.07253
C	-3.15216	-0.72673	0.55456
C	-1.94380	0.19684	0.64515
O	-2.06150	1.41131	0.84620
N	-0.75748	-0.41449	0.53868
H	-11.42324	-2.13523	-1.65342
H	-9.46749	-0.74318	1.68645
H	-9.14511	-0.99040	-2.64678
H	-7.24369	0.05702	-2.31591
H	-5.87646	2.47642	0.12042
H	-6.63952	3.06157	-1.36288
H	-3.63104	3.03031	-0.80566
H	-3.89111	5.49445	-0.60982
H	-4.88925	4.66160	0.59670
H	-5.63812	5.33838	-0.86097
H	-5.22473	4.16819	-3.16405
H	-4.02955	2.86085	-3.25433
H	-3.51134	4.49994	-2.85486
H	-5.13953	0.08417	0.67333
H	-2.91529	-1.58305	-0.08368
H	-3.35703	-1.10078	1.56046
H	-5.50227	1.32494	-2.68460
H	-0.69322	-1.40399	0.34127
H	0.09382	0.12044	0.65344

5. Drug-like parameters

Considering the parameters originally proposed by Lipinski's/Pfizer's rule of five,[2] better absorption or permeation is more likely when molecular weight (MW) is no more than 500 Da, the calculated logP (clogP) does not exceed 5, the number of H-bond acceptors (HBA) and H-bond donors (HBD) are no more than 10 and 5, respectively.[2] Veber's parameters were later introduced and have been found to better discriminate between compounds that are orally active and those that are not for a large data set of compounds in the rat.[3] These parameters include the number of rotatable bonds (n_{rotb}) and the polar surface area (PSA), which should not exceed 10 and 140 Å^2, respectively.[3] Considering these parameters, the drug-like properties for MIF-1 and peptidomimetics **4a** and **6a** were calculated using Molinspiration [http://www.molinspiration.com]. This cheminformatics software is highly useful for predicting the various properties of bioactive peptides and the results are relatable to QSAR studies.[4] The results are listed in **Table S4**.

Table S4. Calculated drug-like properties for MIF-1 and peptidomimetics **4a** and **6a**. [a]Properties calculated using cheminformatics software [http://www.molinspiration.com]. [b]*In silico* BBB permeability using cheminformatics software [http://admet.scbdd.com/calcpre/index/], Category 0: BBB−; Category 1: BBB+; BB ratio ≥ 0.1: BBB+; BB ratio <0.1: BBB−.

Compd	MW[a]	clogP[a]	HBA[a]	HBD[a]	*n*rotb[a]	[t]PSA[a] / Å^2	BB ratio[b]
4a	296.32	0.69	7	2	8	97.64	0.991
6a	281.31	−0.45	7	4	7	114.43	0.984
MIF-1	284.36	−0.93	7	5	7	113.32	0.847
CNS^{+5}	≤ 500	≤ 5	≤ 10	≤ 5	≤ 10	≤ 140	

Accordingly to the Lipinski's/Pfizer's rule of five (**Table S4**), no violations were found for peptidomimetics **4a** and **6a** or MIF-1 neuropeptide. While the number of HBA are the same for **4a**, **6a**, and MIF-1, both peptidomimetics display less HBD than the parent peptide, which may indicate better permeation. As expected, the presence of **3-Fu** as a Pro surrogate and the reduced number of HBD of 3-furoyl derivatives result in higher clogP (0.69 for **4a** and −0.45 for **6a**), which compares favourably with the parent neuropeptide (clogP = −0.93), within the range of adequate CNS$^+$ clogP (≤ 5).

Considering the Veber's parameters (**Table S4**), **4a** displays higher n_{rotb} than **6a** and MIF-1 (n_{rotb} = 8), which may reduce its permeability. Topological polar surface area (^{t}PSA) was used instead of PSA, which provides results of practically the same quality as the classical 3D PSA, however, the calculations are two to three orders of magnitude faster.[6] Molecules with high ^{t}PSA (> 140 A^2) tend to display a low ability to permeate cell membranes.[7] For molecules intended to cross the blood-brain barrier (BBB), a PSA less than 90 $Å^2$ is usually needed,[8] ideally in the range of 60-70 $Å^2$.[7, 8] Among the MIF-1 derivatives, **4a** exhibits the best ^{t}PSA (97.64 $Å^2$), while **6a** and MIF-1 have comparable ^{t}PSA prediction (114.43 and 113.32 $Å^2$, respectively). Nonetheless, all the compounds display ^{t}PSA predictions within the limits (< 140 $Å^2$).

In silico blood-brain (BB) permeation experiments were also performed to determine the probabilities of peptidomimetics to cross the BBB. The results are listed in **Table S4**. BB permeation experiments show that all the tested compounds are considered BBB+ (BB ratio ≥ 0.1). Remarkably, peptidomimetics **4a** and **6a** display better BB permeation (BB ratios of 0.991 and 0.984 for **4a** and **6a**, respectively) than MIF-1 neuropeptide (BB ratio of 0.847). These results are in line with the superior lipophilic character observed for **4a** and **6a** in comparison with MIF-1. A close inspection of the BBB permeation data shows that the replacement of Pro in the MIF-1 structure by **3-Fu** (peptidomimetic **6a**) leads to a pronounced effect on the BB permeability. Peptidomimetics **4a** and **6a** are thus considered to be within the "drug-like" limits and are expected to show enhanced BBB permeation profiles than the parent neuropeptide.

6. Cytotoxicity evaluation of peptidomimetics 4a and 6a in hAd-MSCs

3-Furoyl-based peptidomimetics display no cytotoxicity in hAd-MSCs

The human adipose mesenchymal stem cells (hAd-MSCs) are widely used as *in vitro* models for cytotoxicity studies.[9] In this regard, peptidomimetics **4a** and **6a** were screened on hAd-MSCs. In this assay, cell viability is estimated based on the ability of viable cells to reduce the tetrazolium compound 3-(4,5-dimethylthiazol-2-yl)-5-(3-carboxymethoxyphenyl)-2-(4-sulfophenyl)-2*H* tetrazolium (MTS, inner salt) into the corresponding formazan derivative by functional mitochondrial enzymes.[1] The results of the cytotoxicity assay (MTS) on hAd-MSC are depicted in **Figure S53**. The results obtained show no cytotoxic effect of **4a** and **6a** in the range of concentrations tested. The results demonstrate that these compounds are considered non-cytotoxic up to 0.02 mg mL^{-1}.

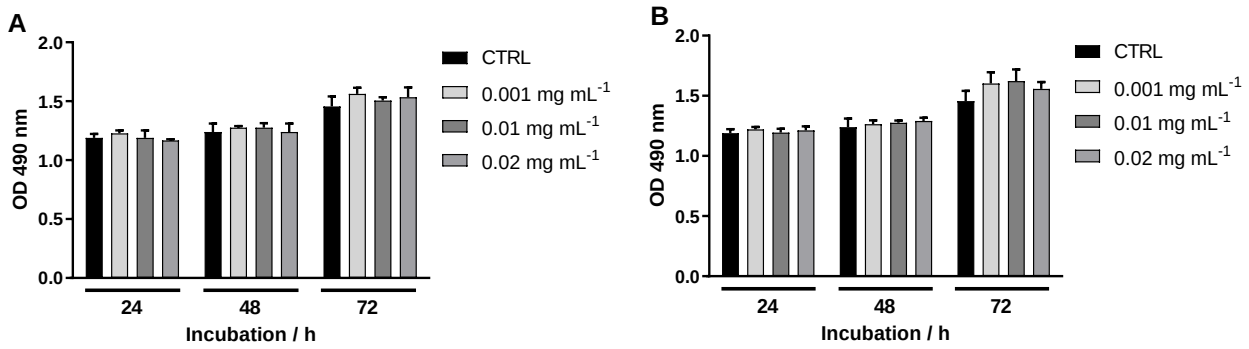

Figure S53. Cell viability of hAd-MSCs tested by the MTS assay, where viable cells were quantified by measuring the OD_{490} of sample wells. hAd-MSCs were treated with peptidomimetics **4a** (**A**) and **6a** (**B**) at different concentrations (0, 0.001, 0.01 and 0.02 mg mL^{-1}) for 72 h. The results were obtained from four wells and three independent experiments and values are presented as mean ± standard deviation. Statistical analyses were performed using One Way Analysis of Variance (ANOVA) test with the previous Shapiro-Wilk normality test. No statistically significant differences were found either between the different concentrations tested or with the control (CTRL).

Methods

Cytotoxicity in hAd-MSC cell culture

To study the cytotoxicity effect of **4a** and **6a**, human adipose mesenchymal stem cells (hAd-MSCs) were used and the CellTiter 96 AQueous (Promega) cell proliferation assay (MTS assay) performed. hAd-MSCs were maintained in Dulbecco´s Modified Eagle's Medium (D6546 Sigma Aldrich, Spain) supplemented with 10% (v/v) fetal bovine serum (FBS, F7524 Sigma Aldrich, Spain) at 37°C in a humidified atmosphere of 5% carbon dioxide (CO_2). Cells were seeded at a density of 5×10^3 cells per 100 µL in 96-well plates and incubated for 24, 48, and 72 h with increasing concentrations (0.001, 0.01, and 0.02 mg/mL) of the peptidomimetics dissolved in the standard culture medium. For control condition, cells were incubated for the same times with standard culture medium. After the different times of incubation, 20 µL of MTS was added to each well followed by 3 h of incubation in dark at 37 °C. Subsequently, the optical density (OD) was read on a multi-well microplate reader at 490 nm. The OD value is directly proportional to the number of metabolic active living cells, so higher OD values indicate a greater number of cells and less cytotoxicity of the compounds.

7. References

1. Sampaio-Dias, I. E.; Silva-Reis, S. C.; García-Mera, X.; Brea, J.; Loza, M. I.; Alves, C. S.; Algarra, M.; Rodríguez-Borges, J. E. Synthesis, pharmacological, and biological evaluation of MIF-1 picolinoyl peptidomimetics as positive allosteric modulators of D_2R. *ACS Chem. Neurosci.* **2019,** 10, 3690-3702.
2. Lipinski, C. A.; Lombardo, F.; Dominy, B. W.; Feeney, P. J. Experimental and computational approaches to estimate solubility and permeability in drug discovery and development settings. *Adv. Drug Delivery Rev.* **1997,** 23, 3-25.
3. Veber, D. F.; Johnson, S. R.; Cheng, H.-Y.; Smith, B. R.; Ward, K. W.; Kopple, K. D. Molecular properties that influence the oral bioavailability of drug candidates. *J. Med. Chem.* **2002,** 45, 2615-2623.
4. Balgir, P. P.; Sharma, M. Biopharmaceutical potential of ACE-inhibitory peptides. *J. Proteomics Bioinform.* **2017,** 10, 171-177.
5. Saitton, S.; Del Tredici, A. L.; Mohell, N.; Vollinga, R. C.; Boström, D.; Kihlberg, J.; Luthman, K. Design, synthesis and evaluation of a PLG tripeptidomimetic based on a pyridine scaffold. *J. Med. Chem.* **2004,** 47, 6595-6602.
6. Ertl, P.; Rohde, B.; Selzer, P. Fast calculation of molecular polar surface area as a sum of fragment-based contributions and its application to the prediction of drug transport properties. *J. Med. Chem.* **2000,** 43, 3714-3717.
7. Pajouhesh, H.; Lenz, G. R. Medicinal chemical properties of successful central nervous system drugs. *NeuroRX* **2005,** 2, 541-553.
8. Hitchcock, S. A.; Pennington, L. D. Structure−brain exposure relationships. *J. Med. Chem.* **2006,** 49, 7559-7583.
9. Efe, B.; Galata, Y. F.; Arslan, Y. E. Assessment of the cytotoxicity of Melia azedarach L. extracts on human adipose-derived mesenchymal stem cells. *Hacettepe J. Biol. Chem.* **2018,** 46, 121-128.